Communications in Advanced Mathematical Sciences

VOLUME IX
ISSUE II

ISSN 2651-4001

VOLUME 9 ISSUE 2
ISSN 2651-4001

June 2026
www.dergipark.org.tr/en/pub/cams

COMMUNICATIONS IN ADVANCED MATHEMATICAL SCIENCES

Indexing and Abstracting

DOAJ

EBSCO Central & Eastern European Academic Source

EBSCO Applied Science & Technology Source Ultimate

Contents

Research Article

1 **Asymptotic Eigenvalue Analysis for a Conformable Fractional Sturm–Liouville Problem**
Olgun Cabri, Suayip Toprakseven 50–59

2 **Chemical Reaction Effects on MHD Convective Flow of a Couple-Stress Fluid Past a Porous Plate Embedded in a Porous Medium**
Deepak Kumar, Mithilesh Kumar Mishra 60–76

3 **Jacobsthal Trees and Generalized $\kappa \cdot x \pm 1$ Transformations**
Petro Kosobutskyy, David Mailland 77–91

Communications in Advanced Mathematical Sciences
ISSN (Online) 2651-4001

Vol. 9, No. 2, 50-59, 2026
https://doi.org/10.33434/cams.1905855
Research Article

Asymptotic Eigenvalue Analysis for a Conformable Fractional Sturm–Liouville Problem

Olgun Cabri[1], Suayip Toprakseven[2]*

Abstract
This paper is devoted to the study of a Sturm–Liouville problem governed by the conformable fractional derivative of order $\alpha \in (0,1]$. We establish the asymptotic behavior of the corresponding eigenvalues subject to appropriate boundary conditions. Through the construction of suitable fundamental solutions and a detailed analysis of the associated characteristic equation, explicit asymptotic eigenvalue formulas are obtained. These results elucidate the influence of the conformable fractional operator on the classical spectral properties and lay a solid analytical foundation for further studies of conformable fractional Sturm–Liouville theory.

Keywords: Conformable fractional derivative, Sturm–Liouville problem, Fractional eigenvalues, Asymptotic analysis, Fundamental solutions

[1] *Department of Business Management, Artvin Çoruh University, Artvin, Türkiye*
[2] *Department of Mathematics, Yozgat Bozok University, Yozgat, Türkiye, suayip.toprakseven@bozok.edu.tr, topraksp@artvin.edu.tr*
Received: 09 March 2026, **Accepted:** 29 April 2026, **Available online:** 21 May 2026
How to cite this article: O. Cabri, S. Toprakseven, *Asymptotic eigenvalue analysis for a conformable fractional Sturm–Liouville problem*, Commun. Adv. Math. Sci., 9(2) (2026), 50-59.

1. Introduction

Fractional differential equations have attracted significant attention over the past decades due to their ability to model memory and hereditary effects arising in various areas of science and engineering, including viscoelasticity, anomalous diffusion, control theory, and signal processing. In particular, fractional operators provide a powerful extension of classical differential models by incorporating nonlocal behavior, which cannot be adequately captured by integer-order derivatives.

Among the various definitions of fractional derivatives, the *conformable fractional derivative*, introduced in [1], has emerged as a promising alternative that preserves many fundamental properties of classical calculus, such as the product rule, chain rule, and mean value theorem. Subsequent studies, including [2–4], have further developed the theoretical foundations of conformable fractional calculus and demonstrated its effectiveness in analytical and numerical investigations.

Sturm–Liouville theory constitutes a cornerstone of mathematical physics and spectral theory, playing a crucial role in the analysis of boundary value problems, eigenfunction expansions, and partial differential equations. Classical Sturm–Liouville problems have been extensively studied and are known to possess well-established spectral properties, including the discreteness, reality, and asymptotic distribution of eigenvalues [5–7], Levitan and Sargsjan [8], and Naimark [9]. Moreover, conformable fractional calculus has been successfully applied to the modeling of complex phenomena arising in science and engineering, particularly in differential equations and applied mathematical models.

In recent years, there has been growing interest in extending Sturm–Liouville theory to fractional-order settings in order to better describe complex physical phenomena. Several authors have investigated fractional Sturm–Liouville problems involving Caputo, Riemann–Liouville, and other nonlocal fractional derivatives; however, these formulations often lead to substantial analytical difficulties due to their inherent nonlocality [10–12].

The conformable fractional derivative provides a more tractable framework for extending Sturm–Liouville theory while preserving a close connection with the classical case. Owing to these advantages, conformable fractional Sturm–Liouville problems have attracted increasing attention in recent years. In particular, fundamental aspects such as the existence and uniqueness of solutions, spectral properties of eigenvalues, self-adjointness of the associated operator, Green's function, and eigenfunction expansions have been investigated in the literature. However, the asymptotic behavior of eigenvalues in the conformable fractional setting remains relatively unexplored, despite its significance in both theoretical analysis and practical applications [13]. Motivated by these foundational results, the present paper focuses on a different but complementary aspect, namely the asymptotic behavior of eigenvalues. More precisely, our main contribution is the derivation of explicit asymptotic formulas for the eigenvalues under appropriate boundary conditions. To the best of our knowledge, such asymptotic eigenvalue characterizations have not been established in explicit form for the considered conformable fractional Sturm–Liouville problem.

The principal aim of this study is to analyze the asymptotic behavior of the eigenvalue spectrum corresponding to a Sturm–Liouville problem defined in terms of the conformable fractional derivative of order $\alpha \in (0,1]$. By constructing appropriate fundamental solutions and performing a careful analysis of the resulting characteristic equation, we derive explicit asymptotic formulas for the eigenvalues. Our results reveal how the conformable fractional structure modifies the classical spectral behavior and reduce to the well-known integer-order case when $\alpha = 1$.

The findings presented in this work contribute to a deeper understanding of conformable fractional Sturm–Liouville problems and provide a rigorous analytical foundation for future studies, including inverse spectral problems, numerical approximations, and applications to fractional partial differential equations.

2. Preliminaries

In this section, we briefly recall the basic concepts and definitions of conformable fractional calculus that will be used throughout the paper. We restrict our attention to conformable derivatives of order $\alpha \in (0,1]$ and summarize only those properties that are essential for the spectral analysis of the associated Sturm–Liouville problem.

Definition 2.1. *Let $f : [0,\infty) \to \mathbb{R}$ be a function and let $\alpha \in (0,1)$. The conformable fractional derivative of f of order α at a point $t > 0$ is defined by*

$$T_\alpha f(t) = \lim_{\varepsilon \to 0} \frac{f(t+\varepsilon t^{1-\alpha}) - f(t)}{\varepsilon},$$

provided that the limit exists. If the limit $\lim_{t\to 0^+} T_\alpha f(t)$ exists, we define

$$T_\alpha f(0) := \lim_{t\to 0^+} T_\alpha f(t).$$

If f is differentiable, then the conformable derivative admits the representation

$$T_\alpha f(t) = t^{1-\alpha} f'(t),$$

which shows that the conformable derivative can be viewed as a weighted version of the classical derivative.

Lemma 2.2. *[1,4] Assume that u and v admit the conformable derivative T_α of order $\alpha \in (0,1)$ at a point $x > 0$. Then:*

(a) *For any constants $\mu, \nu \in \mathbb{R}$,*

$$T_\alpha(\mu u + \nu v) = \mu\, T_\alpha u + \nu\, T_\alpha v.$$

(b) *If u is classically differentiable at x, then*

$$T_\alpha u(x) = x^{1-\alpha} u'(x).$$

(c)

$$T_\alpha(uv)(x) = u(x)\, T_\alpha v(x) + v(x)\, T_\alpha u(x).$$

(d) *If $v(x) \neq 0$, then*

$$T_\alpha\left(\frac{u}{v}\right)(x) = \frac{v(x)\,T_\alpha u(x) - u(x)\,T_\alpha v(x)}{v(x)^2}.$$

(e) *If τ is differentiable, then*

$$T_\alpha\left(e^{\tau(x)}\right) = x^{1-\alpha}\,\tau'(x)\,e^{\tau(x)}.$$

In particular, for $\tau(x) = x^\alpha/\alpha$ one has

$$T_\alpha\left(e^{\tau(x)}\right) = e^{\tau(x)}.$$

All these identities follow directly from the definition of the conformable derivative; see, for instance, [1, 4].

Definition 2.3. *The second conformable derivative of a function f is defined sequentially by*

$$T_\alpha^2 f(t) := T_\alpha\big(T_\alpha f\big)(t),$$

whenever the expression is well defined.

Definition 2.4. *Integrals associated with the conformable derivative are understood with respect to the conformable measure*

$$d_\alpha x := x^{\alpha-1}\,dx.$$

Accordingly, for a suitable function f, the conformable integral is defined by

$$\int_0^x f(\xi)\,d_\alpha\xi = \int_0^x f(\xi)\,\xi^{\alpha-1}\,d\xi.$$

Let u and v be functions defined on $[a,b]$ which admit conformable derivatives of order $\alpha \in (0,1]$. Then the following integration by parts formula holds:

$$\int_a^b u(t)\,T_\alpha v(t)\,d_\alpha t + \int_a^b v(t)\,T_\alpha u(t)\,d_\alpha t = u(b)v(b) - u(a)v(a).$$

We denote by $L^2_\alpha(a,b)$ the space of all complex-valued measurable functions u defined on $[a,b]$ such that

$$\int_a^b |u(t)|^2\,d_\alpha t < \infty.$$

Endowed with the norm

$$\|u\|_{L^2_\alpha} = \left(\int_a^b |u(t)|^2\,d_\alpha t\right)^{1/2},$$

the space $L^2_\alpha(a,b)$ forms a Hilbert space.

3. Problem Statement

We investigate a spectral boundary value problem associated with a second–order conformable fractional differential operator. Specifically, consider the eigenvalue problem

$$T_\alpha^2 y(x) + q(x)\,y(x) = \lambda\,y(x), \qquad x \in (0,1], \tag{3.1}$$

where T_α denotes the conformable fractional derivative of order $\alpha \in (0,1]$, $\lambda \in \mathbb{C}$ is the spectral parameter, and the potential function $q \in C[0,1]$ may be complex–valued. The solution is required to satisfy the separated boundary conditions

$$\begin{aligned} a\,y(0) + b\,T_\alpha y(0^+) &= 0,\\ c\,y(1) + d\,T_\alpha y(1) &= 0, \end{aligned}$$

where $a,b,c,d \in \mathbb{R}$ are prescribed constants not all vanishing simultaneously at each endpoint.

For $\alpha < 1$, the conformable derivative at $x = 0$ is defined whenever the limit exists. We define the solution space as

$$H^1_\alpha(0,1) = \{y \in L^2(0,1) : T_\alpha y \in L^2(0,1),\ \lim_{x\to 0^+} T_\alpha y(x) \text{ exists}\}.$$

Throughout the paper, the potential $q(x)$ in (3.1) is assumed to belong to $L^1(0,1)$.

Lemma 3.1. *Let $q \in C[0,1]$ and $s \in \mathbb{C}\setminus\{0\}$. Consider the nonhomogeneous conformable fractional differential equation*

$$T^2_\alpha y(x) + s^2 y(x) = q(x)\,y(x), \qquad x \in [0,1], \tag{3.2}$$

where T_α denotes the conformable derivative of order $\alpha \in (0,1]$. Then every solution of (3.2) admits the integral representation

$$\begin{aligned} y(x) &= c_1\, e^{\mathrm{i}s\,\tau(x)} + c_2\, e^{-\mathrm{i}s\,\tau(x)} \\ &\quad + \int_0^x \frac{\mathrm{i}}{2s}\left(e^{\mathrm{i}s(\tau(x)-\tau(\xi))} - e^{-\mathrm{i}s(\tau(x)-\tau(\xi))}\right) q(\xi)\,y(\xi)\,d_\alpha\xi, \end{aligned}$$

where $c_1, c_2 \in \mathbb{C}$ are arbitrary constants,

$$\tau(x) := \frac{x^\alpha}{\alpha}, \qquad d_\alpha\xi := \xi^{\alpha-1}\,d\xi.$$

Proof. We begin with the associated homogeneous equation

$$T^2_\alpha y(x) + s^2 y(x) = 0. \tag{3.3}$$

With the substitution $\tau(x) = x^\alpha/\alpha$, the conformable operator $T_\alpha = x^{1-\alpha} d/dx$ is transformed into the ordinary derivative with respect to τ, so that equation (3.3) reduces to a second order equation with constant coefficients, whose fundamental solutions are $e^{\pm is\tau(x)}$. Therefore, the fundamental solutions of (3.3) are given by

$$y_1(x) = e^{is\tau(x)}, \qquad y_2(x) = e^{-is\tau(x)}, \quad \tau(x) = \frac{x^\alpha}{\alpha}.$$

The conformable Wronskian of y_1 and y_2 is defined by

$$W_\alpha(x) = y_1(x) T_\alpha y_2(x) - T_\alpha y_1(x)\, y_2(x),$$

and a direct computation yields

$$W_\alpha(x) = -2is.$$

Applying the method of variation of parameters, a particular solution of the nonhomogeneous equation can be written as

$$y_p(x) = \frac{1}{W_\alpha(x)}\left[y_1(x)\int_0^x y_2(\xi)q(\xi)y(\xi)\,d_\alpha\xi - y_2(x)\int_0^x y_1(\xi)q(\xi)y(\xi)\,d_\alpha\xi\right].$$

Substituting the explicit forms of $y_1(x)$, $y_2(x)$, and $W_\alpha(x)$, we obtain

$$y_p(x) = \frac{1}{2is}\left[e^{is\tau(x)}\int_0^x e^{-is\tau(\xi)}q(\xi)y(\xi)\,d_\alpha\xi - e^{-is\tau(x)}\int_0^x e^{is\tau(\xi)}q(\xi)y(\xi)\,d_\alpha\xi\right].$$

Ultimately, the solution of the nonhomogeneous conformable fractional differential equation can be expressed as the superposition of its complementary (homogeneous) and particular components, yielding the general solution

$$y(x) = c_1 e^{is\tau(x)} + c_2 e^{-is\tau(x)} + \frac{1}{2is}\int_0^x \left(e^{is(\tau(x)-\tau(\xi))} - e^{-is(\tau(x)-\tau(\xi))}\right) q(\xi)y(\xi)\,d_\alpha\xi,$$

where $c_1, c_2 \in \mathbb{C}$ are constants determined by the boundary conditions. $\square$

4. Conformable Integral Representation of the Solution

In this section, we derive an integral representation for solutions of the nonhomogeneous conformable fractional Sturm–Liouville equation. By employing the method of variation of parameters, the differential problem is transformed into an equivalent Volterra–type integral equation. This formulation plays a central role in the subsequent asymptotic analysis of the eigenvalues and eigenfunctions.

Let $s \in \mathbb{C}$ be the spectral parameter and recall that $\tau(x) = x^{\alpha}/\alpha$ and $d_{\alpha}\xi = \xi^{\alpha-1}d\xi$. A solution of the equation

$$T_{\alpha}^{2}y(x) + s^{2}y(x) = q(x)y(x), \qquad x \in (0,1],$$

admits the integral representation;

$$y(x) = c_1 e^{is\tau(x)} + c_2 e^{-is\tau(x)} + \int_0^x \frac{ie^{is(\tau(x)-\tau(\xi))} - ie^{-is(\tau(x)-\tau(\xi))}}{2s} q(\xi)y(\xi)\,d_{\alpha}\xi,$$

where $c_1, c_2 \in \mathbb{C}$ are constants determined by the boundary conditions.

For later convenience, we introduce modified constants

$$c_j' = \begin{cases} c_1, & j=1, \\ c_2 + \displaystyle\int_0^1 \frac{-ie^{-is\tau(\xi)}}{2s} q(\xi)y(\xi)\,d_{\alpha}\xi, & j=2, \end{cases}$$

which allow the solution to be written in the symmetric form

$$\begin{aligned} y(x) &= c_1' e^{is\tau(x)} + c_2' e^{-is\tau(x)} \\ &\quad + \frac{1}{2s}\int_0^x K_1(x,\xi,s)\,q(\xi)y(\xi)\,d_{\alpha}\xi - \frac{1}{2s}\int_x^1 K_2(x,\xi,s)\,q(\xi)y(\xi)\,d_{\alpha}\xi. \end{aligned}$$

The kernel functions are defined by

$$K_1(x,\xi,s) = ie^{is(\tau(x)-\tau(\xi))}, \qquad K_2(x,\xi,s) = ie^{-is(\tau(x)-\tau(\xi))}. \tag{4.1}$$

Lemma 4.1. *There exists a constant $C>0$ such that for all s belonging to a fixed region T of the complex plane, the following estimates hold:*

$$\begin{aligned} &\left|T_{\alpha}^{\nu}K_1(x,\xi,s)\right| \le C|s|^{\nu}\left|e^{is(\tau(x)-\tau(\xi))}\right|, \qquad 0<\xi<x<1, \\ &\left|T_{\alpha}^{\nu}K_2(x,\xi,s)\right| \le C|s|^{\nu}\left|e^{-is(\tau(x)-\tau(\xi))}\right|, \qquad 0<x<\xi<1, \end{aligned}$$

for $\nu = 0,1,2$.

Proof. Let $s \in T \subset \mathbb{C}$, where T is a fixed region. Since τ is monotone on $(0,1]$, there exists a constant $C>0$ such that

$$\left|e^{is(\tau(x)-\tau(\xi))}\right| \le C, \qquad x,\xi \in [\delta,1], \quad 0<\delta<1.$$

Assume further that s satisfies the sectorial condition

$$\Re(is(\tau(x)-\tau(\xi))) \le -c(\tau(x)-\tau(\xi)), \qquad x>\xi,\ c>0,$$

which implies

$$\left|e^{is(\tau(x)-\tau(\xi))}\right| \le e^{-c(\tau(x)-\tau(\xi))}.$$

Using the definition of the conformable derivative, we compute

$$T_{\alpha}^{\nu}K_1(x,\xi,s) = x^{\nu(1-\alpha)}(is)^{\nu}\left(\tau'(x)\right)^{\nu}e^{is(\tau(x)-\tau(\xi))}, \qquad \nu = 0,1,2.$$

Since $\tau'(x) = x^{\alpha-1}$, it follows that

$$\left|T_{\alpha}^{\nu}K_1(x,\xi,s)\right| \le C|s|^{\nu}\left|e^{is(\tau(x)-\tau(\xi))}\right|,$$

uniformly for $x,\xi \in [\delta,1]$. The estimate for K_2 is obtained analogously. □

The integral representation established in Lemma 3.1 allows the conformable fractional equation to be recast as a Volterra-type integral equation whose kernel depends parametrically on the complex spectral parameter s. This formulation is particularly well suited for the analysis of the large–$|s|$ regime, since the oscillatory exponential terms associated with the homogeneous problem dominate the contribution of the potential $q(x)$. As in the classical Sturm–Liouville theory, one therefore expects the high-frequency behavior of solutions to be governed primarily by the principal part of the operator, with $q(x)$ producing only lower-order perturbations.

By combining successive approximations of the Volterra equation with standard estimates for oscillatory integrals in the conformable setting, one can construct a fundamental system of solutions that is analytic in the spectral parameter and admits explicit asymptotic expansions. The following theorem makes this statement precise and provides uniform high-energy asymptotics for the conformable fractional equation.

Theorem 4.2 (High–frequency asymptotics)**.** *Let $q \in C[0,1]$. For any fixed region T of the complex s–plane, the conformable fractional differential equation*

$$T_\alpha^2 y(x) + s^2 y(x) = q(x)\,y(x), \qquad x \in (0,1],$$

admits a fundamental system of two linearly independent solutions $\{y_1, y_2\}$ that are analytic with respect to $s \in T$ for sufficiently large $|s|$. Moreover, as $|s| \to \infty$, these solutions satisfy the uniform asymptotic expansions

$$y_k(x) = e^{s\omega_k \tau(x)}\left(1 + \mathscr{O}\left(|s|^{-1}\right)\right), \tag{4.2}$$

$$T_\alpha y_k(x) = s\omega_k\, e^{s\omega_k \tau(x)}\left(1 + \mathscr{O}\left(|s|^{-1}\right)\right), \tag{4.3}$$

$$T_\alpha^2 y_k(x) = s^2 \omega_k^2\, e^{s\omega_k \tau(x)}\left(1 + \mathscr{O}\left(|s|^{-1}\right)\right), \tag{4.4}$$

where $\omega_1 = i$, $\omega_2 = -i$, and $\tau(x) = x^\alpha/\alpha$. The above estimates hold uniformly for $x \in [\delta, 1]$ and $s \in T$, for any fixed $\delta \in (0,1)$.

Proof. Let $\delta \in (0,1)$ be fixed and consider $x \in [\delta, 1]$ and $s \in T$, where T is a fixed region in the complex plane.

By Lemma 3.1, for each $k \in \{1,2\}$ there exists a solution y_k of

$$T_\alpha^2 y + s^2 y = q(x)\,y,$$

which admits the integral representation

$$y_k(x) = e^{s\omega_k \tau(x)} + \frac{1}{2s}\int_0^x K_1(x,\xi,s)\,q(\xi)\,y_k(\xi)\,d_\alpha \xi - \frac{1}{2s}\int_x^1 K_2(x,\xi,s)\,q(\xi)\,y_k(\xi)\,d_\alpha \xi, \tag{4.5}$$

where K_1 and K_2 are the conformable kernels defined in (4.1).

By Lemma 4.1, for each $\nu = 0,1,2$, the quantities $T_\alpha^\nu K_j(x,\xi,s)$ are continuous and uniformly bounded. Applying T_α^ν to (4.5) yields, for $\nu = 0,1,2$,

$$\begin{aligned} T_\alpha^\nu y_k(x) = s^\nu \omega_k^\nu e^{s\omega_k \tau(x)} &+ \frac{1}{2s}\int_0^x T_\alpha^\nu K_1(x,\xi,s)\,q(\xi)\,y_k(\xi)\,d_\alpha \xi \\ &- \frac{1}{2s}\int_x^1 T_\alpha^\nu K_2(x,\xi,s)\,q(\xi)\,y_k(\xi)\,d_\alpha \xi. \end{aligned} \tag{4.6}$$

For $\nu = 0,1$, define the normalized functions

$$z_\nu(x,s) := T_\alpha^\nu\left(e^{-s\omega_k \tau(x)} y_k(x)\right).$$

Multiplying (4.6) by $e^{-s\omega_k \tau(x)}$ and using $y_k(\xi) = e^{s\omega_k \tau(\xi)} z_0(\xi,s)$, we obtain

$$z_\nu(x,s) = \omega_k^\nu + \frac{1}{s}\int_0^1 K_{k\nu}(x,\xi,s)\,q(\xi)\,z_0(\xi,s)\,d_\alpha \xi, \quad \nu = 0,1, \tag{4.7}$$

where the kernel $K_{k\nu}$ is defined piecewise by

$$K_{k\nu}(x,\xi,s) := \begin{cases} \frac{1}{2} e^{-s\omega_k(\tau(x)-\tau(\xi))} T_\alpha^\nu K_1(x,\xi,s), & 0 \le \xi < x, \\ -\frac{1}{2} e^{-s\omega_k(\tau(x)-\tau(\xi))} T_\alpha^\nu K_2(x,\xi,s), & x < \xi \le 1. \end{cases}$$

In particular, by Lemma 4.1 and the uniform boundedness of the exponential terms on $[\delta,1]\times[\delta,1]$ for $s\in T$, there exist constants $C_\nu = C_\nu(\delta,T)>0$ such that

$$\sup_{x\in[\delta,1]} |K_{k\nu}(x,\xi,s)| \le C_\nu, \quad \forall \xi\in[0,1],\ s\in T,\ \nu=0,1. \tag{4.8}$$

Let

$$m_0(s) := \max_{x\in[\delta,1]} |z_0(x,s)|.$$

Then, from (4.7) and (4.8), we have

$$\begin{aligned} |z_0(x,s)| &\le 1+\frac{C_0}{|s|}\int_0^1 |q(\xi)|\,|z_0(\xi,s)|\,d_\alpha\xi \\ &\le 1+\frac{C_0}{|s|}\left(\int_0^1 |q(\xi)|\,d_\alpha\xi\right) m_0(s) \\ &= 1+\frac{A}{|s|}m_0(s), \quad A := C_0\int_0^1 |q(\xi)|\,d_\alpha\xi. \end{aligned}$$

For $|s|>2A$, the preceding inequality implies

$$m_0(s)\le 2.$$

Substituting this bound into (4.7) with $\nu=0$, we obtain

$$\begin{aligned} |z_0(x,s)-1| &\le \frac{C_0}{|s|}\int_0^1 |q(\xi)|\,|z_0(\xi,s)|\,d_\alpha\xi \\ &\le \frac{2A}{|s|} = \mathscr{O}\left(\frac{1}{|s|}\right), \end{aligned}$$

uniformly for $x\in[\delta,1]$ and $s\in T$ as $|s|\to\infty$. Hence,

$$z_0(x,s) = 1+\mathscr{O}\left(\frac{1}{|s|}\right), \quad x\in[\delta,1],\ s\in T,\ |s|\to\infty. \tag{4.9}$$

Similarly, from (4.7) with $\nu=1$, the boundedness of z_0, and (4.8), we have

$$\begin{aligned} |z_1(x,s)-\omega_k| &\le \frac{C_1}{|s|}\int_0^1 |q(\xi)|\,|z_0(\xi,s)|\,d_\alpha\xi \\ &\le \frac{2C_1}{|s|}\int_0^1 |q(\xi)|\,d_\alpha\xi = \mathscr{O}\left(\frac{1}{|s|}\right), \end{aligned}$$

uniformly for $x\in[\delta,1]$, $s\in T$, as $|s|\to\infty$. Therefore,

$$z_1(x,s) = \omega_k+\mathscr{O}\left(\frac{1}{|s|}\right), \quad x\in[\delta,1],\ s\in T.$$

Now, recalling that $y_k(x) = e^{s\omega_k\tau(x)}z_0(x,s)$, (4.9) gives

$$y_k(x) = e^{s\omega_k\tau(x)}\left[1+\mathscr{O}\left(\frac{1}{|s|}\right)\right], \quad x\in[\delta,1].$$

Moreover, using $T_\alpha y_k(x) = T_\alpha\left(e^{s\omega_k\tau(x)}z_0(x,s)\right)$ and the definition of z_1, we obtain

$$T_\alpha y_k(x) = e^{s\omega_k\tau(x)}z_1(x,s) = s\omega_k e^{s\omega_k\tau(x)}\left[1+\mathscr{O}\left(\frac{1}{|s|}\right)\right], \quad x\in[\delta,1].$$

Finally, from the differential equation itself, we have

$$T_\alpha^2 y_k(x) = (q(x)-s^2)y_k(x) = s^2\omega_k^2 e^{s\omega_k\tau(x)}\left[1+\mathscr{O}\left(\frac{1}{|s|}\right)\right], \quad x\in[\delta,1],$$

since $\omega_k^2=-1$ for $\omega_k\in\{i,-i\}$ and $q(x)$ is bounded.

For sufficiently large $|s|$, the functions $e^{s\omega_1\tau(x)}$ and $e^{s\omega_2\tau(x)}$ are linearly independent. Equivalently, the associated conformable Wronskian satisfies

$$W_\alpha(y_1,y_2) = -2is\big(1+o(1)\big)\neq 0,$$

which confirms that y_1 and y_2 form a fundamental system of solutions.

Therefore, for each fixed $\delta\in(0,1)$, the asymptotic estimates derived above hold uniformly for $x\in[\delta,1]$ and $s\in T$ as $|s|\to\infty$, which completes the proof.

□

Remark 4.3. *The asymptotic expressions (4.2)–(4.4) show that, for sufficiently large $|s|$, the solutions exhibit oscillatory exponential behavior, with the phase modulated by the conformable time scale $\tau(x)=x^\alpha/\alpha$.*

Theorem 4.4 (Asymptotic Eigenvalues)**.** *Let the conformable fractional Sturm–Liouville problem be subject to the boundary conditions*

$$U_1(y) = a\,y(0)+b\,T_\alpha y(0^+), \qquad U_2(y) = c\,y(1)+d\,T_\alpha y(1),$$

where T_α is the conformable derivative operator and $\tau(x)=x^\alpha/\alpha$. Then, for sufficiently large indices, the eigenvalues admit the asymptotic representation

$$s_k = \frac{\alpha}{\omega_\mu}\big(\ln\xi+2\pi ik\big), \quad k\in\mathbb{Z},$$

and

$$\lambda_k = s_k^2,$$

where ω_μ is a characteristic constant depending on the boundary parameters and ξ is determined by the boundary conditions.

Proof. For brevity, denote

$$[1] := 1+\mathscr{O}\left(\frac{1}{|s|}\right), \quad |s|\to\infty.$$

By Theorem 4.2, the asymptotic forms of the fundamental solutions yield

$$y_k(0)=[1], \qquad T_\alpha y_k(0^+) = s\omega_k[1].$$

Substituting these into the boundary conditions gives

$$U_1(y_k) = a[1]+bs\omega_k[1] = (a+bs\omega_k)[1],$$

$$U_2(y_k) = (c+ds\omega_k)e^{s\omega_k\tau(1)}[1].$$

Hence, the characteristic determinant becomes

$$\begin{aligned}\Delta(s) &= \det\begin{pmatrix}U_1(y_1) & U_1(y_2)\\ U_2(y_1) & U_2(y_2)\end{pmatrix}\\ &= (a+bs\omega_1)(c+ds\omega_2)e^{s\omega_2\tau(1)} - (a+bs\omega_2)(c+ds\omega_1)e^{s\omega_1\tau(1)} + \mathscr{O}\left(\frac{1}{|s|}\right).\end{aligned}$$

Choosing symmetric roots $\omega_1 = \omega_\mu$ and $\omega_2 = -\omega_\mu$, we obtain the characteristic determinant in the form

$$\Delta(s) = \theta_1 e^{-s\omega_\mu \tau(1)} + \theta_{-1} e^{s\omega_\mu \tau(1)} + \mathscr{O}\left(\frac{1}{|s|}\right),$$

for suitable constants $\theta_1, \theta_{-1} \neq 0$. Multiplying both sides by $e^{s\omega_\mu \tau(1)}$ gives

$$e^{s\omega_\mu \tau(1)} \Delta(s) = \theta_1 e^{-2s\omega_\mu \tau(1)} + \theta_{-1} + \mathscr{O}\left(\frac{1}{|s|}\right).$$

Setting $\xi := e^{s\omega_\mu \tau(1)}$, the leading-order characteristic equation reduces to

$$\theta_1 \xi^2 + \theta_{-1} = 0 \quad \Longrightarrow \quad \xi = \pm\sqrt{-\frac{\theta_{-1}}{\theta_1}}.$$

Taking logarithms in the relation $\xi = e^{s\omega_\mu \tau(1)}$ yields

$$s\omega_\mu \tau(1) = \ln \xi.$$

Finally, solving for s yields the asymptotic eigenvalues

$$s_k = \frac{\alpha}{\omega_\mu}\big(\ln \xi + 2\pi i k\big), \quad k \in \mathbb{Z},$$

and the corresponding eigenvalues of the Sturm–Liouville problem are

$$\lambda_k = s_k^2.$$

This completes the proof. □

5. Conclusion

This study concerns a class of conformable fractional Sturm–Liouville problems formulated on a compact interval and subject to general linear endpoint conditions. By exploiting the structural properties of the conformable derivative, the original fractional differential equation was transformed into an equivalent ordinary differential equation through an appropriate change of variables. This transformation enabled the systematic application of classical analytical techniques within a fractional framework.

An explicit integral formulation of the solution is obtained by employing the framework of the Green-function approach, which encodes both the homogeneous dynamics and the effect of the nonhomogeneous forcing term. The resulting Volterra–type integral equation provided a robust analytical tool for studying the qualitative behavior of solutions and served as the foundation for establishing precise asymptotic estimates. Uniform bounds for the associated kernel functions and their conformable derivatives were obtained in suitable regions of the complex spectral plane, ensuring the well-posedness of the integral formulation.

Furthermore, the existence of two linearly independent solutions with well-defined asymptotic behavior was demonstrated. These solutions were shown to admit exponential representations governed by the conformable phase function $\tau(x) = x^\alpha/\alpha$, with error terms that decay uniformly as the spectral parameter tends to infinity. Such asymptotic expansions play a crucial role in the spectral analysis of conformable fractional Sturm–Liouville operators, particularly in the study of eigenvalue distributions and eigenfunction expansions.

The results presented herein extend classical Sturm–Liouville theory to the conformable fractional setting and provide a rigorous analytical framework for future investigations. Potential directions for further research include inverse spectral problems, completeness and basis properties of eigenfunctions, and the development of numerical schemes guided by the derived asymptotic behavior. The methodology developed in this paper may also be adapted to more general classes of fractional operators and boundary conditions.

Article Information

Acknowledgements: The authors would like to express their sincere thanks to the editor and the anonymous reviewers for their helpful comments and suggestions.

Author Contributions: Conceptualization: OC; Methodology: ST; Validation: OC, ST; Formal analysis: OC, ST; Investigation: ST; Writing – original draft: OC, ST; Writing – review & editing: OC, ST; Project administration: ST.

Artificial Intelligence Statement: No artificial intelligence tools were used in the preparation of this manuscript.

Conflict of Interest Disclosure: No potential conflict of interest was declared by authors.

Plagiarism Statement: This article was scanned by the plagiarism program.

References

[1] R. Khalil, M. Al Horani, A. Yousef, et al., *A new definition of fractional derivative,* J. Comput. Appl. Math., **264** (2014), 65–70. https://doi.org/10.1016/j.cam.2014.01.002

[2] A. Atangana, D. Baleanu, *New properties of conformable derivative*, Open Math., **13** (2015), 889–898. https://doi.org/10.1515/math-2015-0081

[3] R. Almeida, *A Caputo fractional derivative of a function with respect to another function*, Commun. Nonlinear Sci. Numer. Simul., **44** (2017), 460–481. https://doi.org/10.1016/j.cnsns.2016.09.006

[4] T. Abdeljawad, *On conformable fractional calculus*, J. Comput. Appl. Math., **279** (2015), 57–66. https://doi.org/10.1016/j.cam.2014.10.016

[5] E. C. Titchmarsh, *Eigenfunction Expansions Associated with Second-Order Differential Equations*, Oxford University Press, Oxford, 1946.

[6] A. Zettl, *Sturm–Liouville Theory*, American Mathematical Society, Providence, RI, 2005.

[7] O. Cabri, S. Toprakseven, *On q Sturm–Liouville operator with periodic boundary conditions*, Contemp. Math., **5**(4) (2024), 4309–4322. https://doi.org/10.37256/cm.5420245208

[8] B. M. Levitan, I. S. Sargsjan, *Sturm–Liouville and Dirac Operators*, Kluwer Academic Publishers, Dordrecht, 1991.

[9] M. A. Naimark, *Linear Differential Operators, Part II*, Frederick Ungar Publishing Co., New York, 1968.

[10] M. Yavuz, N. Özdemir, *On the solutions of fractional Cauchy problem featuring conformable derivative*, ITM Web Conf., **22** (2018), Article ID 01045. https://doi.org/10.1051/itmconf/20182201045

[11] A. Salim, S. Krim, J. E. Lazreg, et al., *A study on some conformable fractional implicit hybrid differential equations with delay*, Kragujevac J. Math., **50**(3) (2026), 439–455. https://doi.org/10.46793/KgJMat2603.439S

[12] C. F. L. Godinho, C. M. Porto, M. C. Rodriguez, et al., *Coherent states of the conformable quantum oscillator*, Dynamics, **5**(3) (2025), Article ID 26. https://doi.org/10.3390/dynamics5030026

[13] B. P. Allahverdiev, H. Tuna, Y. Yalçinkaya, *Conformable fractional Sturm–Liouville equation*, Math. Methods Appl. Sci., **42**(9) (2019), 3508–3526. https://doi.org/10.1002/mma.5595

Communications in Advanced Mathematical Sciences
ISSN (Online) 2651-4001
Vol. 9, No. 2, 60-76, 2026
https://doi.org/10.33434/cams.1883238
Research Article

Chemical Reaction Effects on MHD Convective Flow of a Couple-Stress Fluid Past a Porous Plate Embedded in a Porous Medium

Deepak Kumar[1]*, Mithilesh Kumar Mishra[1]

Abstract
The present paper examines the heat and mass transfer characteristics of convective magnetohydrodynamic (MHD) flow of a couple-stress fluid past a vertical porous plate within a porous medium. The analysis incorporates time-dependent oscillatory suction and permeability, together with the effects of an internal heat source and a first-order chemical reaction. The governing nonlinear partial differential equations are formulated in dimensionless form and separated into steady and oscillatory components. The differential equations are solved numerically, and the variations in velocity, temperature, and concentration distributions are depicted graphically. Additionally, skin friction, the Nusselt number, and the Sherwood number are presented in tables. The study presents the influence of key parameters, including the chemical reaction rate, magnetic field strength, couple-stress parameter, oscillation amplitude of permeability, Prandtl number, Schmidt number, and heat source intensity, to analyse the fluid behaviour.

Keywords: Porous medium, Magnetohydrodynamic (MHD) flow, Couple-stress fluid, Oscillatory permeability

[1] *Babasaheb Bhimrao Ambedkar Bihar University, Bihar, India, deepakmaths@yahoo.com, mithileshmishra0194@gmail.com*
***Corresponding author**

Received: 6 February 2026, **Accepted:** 6 June 2026, **Available online:** 7 June 2026
How to cite this article: D. Kumar, M. K. Mishra, *Chemical reaction effects on MHD convective flow of a couple-stress fluid past a porous plate embedded in a porous medium*, Commun. Adv. Math. Sci., 9(2) (2026), 60-76.

1. Introduction

In recent decades, the study of magnetohydrodynamic (MHD) flow of couple-stress fluid through porous media has attracted many researchers due to its wide applications in geophysical and engineering processes. Couple-stress fluids take into account the occurrence of microscopic rotations and particle-size effects. Therefore, they provide a more realistic description of biological fluids, lubricants, and polymeric suspensions compared to classical Newtonian models. When such fluids flow through a porous medium under the influence of an applied transverse magnetic field, the interplay between viscous, couple stress, magnetic, and drag forces alters the momentum transport characteristics. The chemical reaction influences the concentration field, which affects buoyancy-driven flows and mass transfer rates. Understanding the combined effects of couple stress behaviour, applied magnetic fields, and chemical reactions on flow through a porous medium is essential in designing chemical reactors, filtration systems and biomedical devices where electrically conducting fluids are involved.

Chamkha [1] analysed an unsteady magnetohydrodynamic (MHD) convective heat and mass transfer past a semi-infinite vertical permeable moving plate. Prasad and Reddy [2] studied radiation and mass transfer effects on an unsteady, laminar, hydromagnetic free convection flow past a heated vertical plate in a porous medium with viscous dissipation. Their study highlights the significance of radiation and mass transfer on fluid and heat transfer. Das et al. [3] investigated mass transfer effects on MHD convective flow and heat transfer past a vertical porous plate through a porous medium under oscillatory suction and heat source. They presented an in-depth analysis of the effects of mass transfer on fluid flow and heat transfer. Ram et al. [4] analysed how chemical reactions and heat transfer influence magnetohydrodynamic (MHD) flow of viscous fluid past a moving isothermal vertical porous plate with suction that varies with time. The paper emphasises the impact of chemical reaction on both mass and heat transfer of the fluid flow. Mass transfer effects on MHD unsteady convective Walters's flow with constant suction and a heat sink have been presented by Kumar and Satyanarayana [5]. Rao et al. [6] presented chemical reaction effects on an unsteady MHD free convection fluid flow past a semi-infinite vertical plate embedded in a porous medium with heat absorption, and found that the velocity and concentration decrease with an increase in the Schmidt number. The effects of various flow parameters on velocity, temperature and concentration are presented through graphs, whereas variations in skin friction and the Nusselt number are presented in tables. Shivaiah and Rao [7] analysed the behaviour of an unsteady MHD free convection flow past a vertical porous plate, considering the effects of suction or injection. They discussed how chemical reactions affect the fluid flow and heat transfer. The impact of chemical reaction on an unsteady MHD free convection flow past an infinite vertical porous plate with variable suction has been studied by Sarada and Shanker [8]. Mishra et al. [9] examined the effects of mass and heat transfer on magnetohydrodynamic flow of a visco-elastic fluid through a porous medium with oscillatory suction and heat source. They found that the fluid's elasticity is responsible for the thinning of the boundary layer. The influence of chemical reaction and magnetic fields on a couple-stress fluid over a non-linearly stretching sheet has been studied by Khan et al. [10]. They observed that the concentration of the couple stress decreases as the Schmidt number increases. Nayak et al. [11] explored how chemical reaction influences the magnetohydrodynamic flow of a visco-elastic fluid through a porous medium. Balamurugan et al. [12] studied unsteady MHD free convective flow past a moving vertical plate with time-dependent suction and chemical reaction in a slip flow regime. They noticed that fluid velocity decreases as the radiation parameter, the Prandtl number and the inclined angle parameter increase. Rout et al. [13] examined the impact of chemical reaction on MHD free convection flow of a micro-polar fluid. Unsteady MHD free convective flow of a visco-elastic fluid past an infinite vertical porous moving plate with varying temperature and concentration is discussed by Ramesh Babu et al. [14]. They discovered that the temperature increases as the absorption of radiation parameter increases. Kumaresan et al. [15] obtained an exact solution for the unsteady MHD free convective chemically reacting visco-elastic fluid past a moving vertical plate through a porous medium. Raghunath et al. [16] discussed heat and mass transfer on MHD flow of non-Newtonian fluid over an infinite vertical porous plate. They observed that an increase in the heat absorption coefficient leads to a decrease in temperature, while the opposite effect is noticed when a constant scalar is present. Choudhury and Dey [17] studied thermal radiation effects on MHD convective slip flow of visco-elastic fluid past a porous plate within a porous medium. Kumari and Raju [18] explored unsteady magnetohydrodynamic free convective flow past a vertical porous plate with span-wise fluctuating, heat and mass transfer effects. Arif et al. [19] discussed newly developed fractal-fractional derivatives with a power law kernel for magnetohydrodynamic couple-stress fluid in a channel within a porous medium. Waseem et al. [20] studied gravity-driven hydromagnetic flow of couple stress hybrid nanofluid with both homogeneous and heterogeneous reactions. Mopuri et al. [21] explored MHD flow and heat transfer past a vertical porous plate in the presence of various flow parameters. Ravikumar et al. [22] studied the effects of Joule heating and reaction mechanisms on couple-stress and Jeffrey fluid flows with peristalsis, considering the presence of a porous material within an inclined and tapered channels. Sharma and Jain [23] presented chemical reactions occurring in an MHD couple stress fluid towards a stretchable inclined cylinder. They stated that as the Schmidt number increases, mass diffusivity decreases, leading to a declining concentration profile. Kavitha and Angel [24] investigated the impact of rotation and chemical reaction on mixed convection flow over an inclined heated porous plate. They observed that an increase in the heat source and the radiation parameter leads to a decrease in the temperature distribution. Also, the concentration boundary layer reduces as the Schmidt number and the chemical reaction parameter increase.

The aim of the present study is to explore the effect of variable permeability and oscillatory suction velocity on the convective flow of a couple-stress fluid past an infinite vertical porous plate in a porous medium under the influence of a uniform transverse magnetic field and chemical reactions. Despite extensive research on Newtonian and viscoelastic fluids, the effect of couple-stress fluids in the present situation has not been explored enough. The novelty of this research is the incorporation of couple-stress effects that account for microstructural interactions and lead to significant changes in the flow and transport properties. This study has practical applications in groundwater flows, geothermal problems, the use of chemical fertilizers on soil, and oil extraction processes.

2. Mathematical Formulation

The unsteady free convective flow of a couple-stress fluid past an infinite vertical porous plate within a porous medium, along with the influence of a transverse magnetic field, is considered. The permeability and the suction velocity are time-dependent and oscillatory in nature. Let the x'-axis be aligned with the plate in the direction of the flow, and the y'-axis be normal to it.

The magnetic Reynolds number is considered to be less than unity, so that the induced magnetic field is negligible compared to the applied transverse magnetic field. Therefore, the flow in the medium is entirely due to the buoyancy force caused by the temperature difference between the porous medium and the wall. Initially, for $t' \leq 0$, both the plate and the fluid are at the same temperature, and the concentration of the species is very low. Under these conditions, the Soret and Dufour effects can be neglected. When $t' > 0$, the temperature of the plate is instantaneously raised to T'_w and the concentration of the species is changed to C'_w. Let the time-dependent oscillatory permeability of the porous medium and the suction velocity be of the form

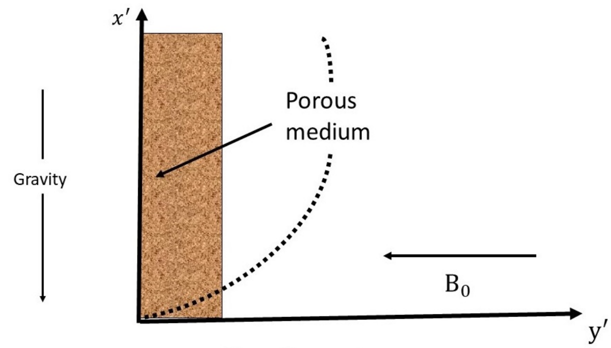

Figure 2.1. Flow diagram.

$$K_p = K'_p\left(1+\varepsilon e^{i\omega' t'}\right), \tag{2.1}$$

$$v(t') = -v_0\left(1+\varepsilon e^{i\omega' t'}\right), \tag{2.2}$$

where $v_0 > 0$ and $\varepsilon \ll 1$ are positive constants. Under the above assumptions and the usual Boussinesq approximation, the governing equations and boundary conditions for the flow are given by

$$\rho\left(\frac{\partial u'}{\partial t'}+v\frac{\partial u'}{\partial y'}\right) = \mu\frac{\partial^2 u'}{\partial y'^2}+\rho g\beta(T'-T_\infty)+\rho g\beta^*(C'-C_\infty)-\sigma B_0^2 u'-\frac{\mu u'}{K'_p(1+\varepsilon e^{i\omega' t'})}-\eta\frac{\partial^4 u'}{\partial y'^4} \tag{2.3}$$

$$\frac{\partial T'}{\partial t'}+v\frac{\partial T'}{\partial y'} = \alpha\frac{\partial^2 T'}{\partial y'^2}+S'(T'-T_\infty) \tag{2.4}$$

$$\frac{\partial C'}{\partial t'}+v\frac{\partial C'}{\partial y'} = D\frac{\partial^2 C'}{\partial y'^2}-K'_c(C'-C_\infty) \tag{2.5}$$

$$\left.\begin{array}{l} u=0, \quad T'=T_w+\varepsilon(T_w-T_\infty)e^{i\omega' t'}, \quad C'=C_w+\varepsilon(C_w-C_\infty)e^{i\omega' t'}, \quad \dfrac{\partial^2 u}{\partial y'^2}=0 \quad \text{at } y=0 \\ u\to 0, \quad T'\to T_\infty, \quad C'\to C_\infty, \quad \dfrac{\partial^2 u}{\partial y'^2}\to 0 \quad \text{as } y\to\infty \end{array}\right\} \tag{2.6}$$

In the boundary layer analysis, we assume μ and η to be of same order of magnitude. This will ensure that both the viscous and couple-stress effects are equally significant in influencing the flow characteristics.

3. Non-Dimensionalization of Flow Quantities

To non-dimensionalize the governing equations and boundary conditions of the flow, the following non-dimensional variables and parameters are introduced.

$$\left.\begin{array}{l} y=\dfrac{u_0 y'\rho}{\mu}, \quad t=\dfrac{u_0^2 t'\rho}{4\mu}, \quad \omega=\dfrac{4\mu\omega'}{u_0^2\rho}, \quad u=\dfrac{u'}{u_0}, \quad T=\dfrac{T'-T_\infty}{T_w-T_\infty}, \quad \phi=\dfrac{\eta u_0^2\rho^2}{\mu^3} \\ C=\dfrac{C'-C_\infty}{C_w-C_\infty}, \quad S=\dfrac{\mu S'}{\rho u_0^2}, \quad K_p=\dfrac{u_0^2 K'_p\rho^2}{\mu^2}, \quad M^2=\dfrac{\sigma B_0^2\mu}{\rho^2 u_0^2}, \quad \mathrm{K}_c=\dfrac{\mu K'_c}{\rho u_0^2} \\ \mathrm{P}_r=\dfrac{\mu}{\rho\alpha}, \quad G_c=\dfrac{\mu g\beta'(C_w-C_\infty)}{\rho u_0^3}, \quad G_r=\dfrac{\mu g\beta(T_w-T_\infty)}{\rho u_0^3}, \quad \mathrm{S}_c=\dfrac{\mu}{\rho D} \end{array}\right\} \tag{3.1}$$

Using non-dimensional parameters (3.1), and the equations (2.1) and (2.2), the governing flow equations and boundary conditions (2.3) to (2.6) reduce to the following non-dimensional form

$$\frac{1}{4}\frac{\partial u}{\partial t} - (1+\varepsilon e^{i\omega t})\frac{\partial u}{\partial y} = \frac{\partial^2 u}{\partial y^2} + G_r T + G_c C - M^2 u - \frac{u}{K_p(1+\varepsilon e^{i\omega t})} - \phi\frac{\partial^4 u}{\partial y^4} \tag{3.2}$$

$$\frac{1}{4}\frac{\partial T}{\partial t} - (1+\varepsilon e^{i\omega t})\frac{\partial T}{\partial y} = \frac{1}{P_r}\frac{\partial^2 T}{\partial y^2} + ST \tag{3.3}$$

$$\frac{1}{4}\frac{\partial C}{\partial t} - (1+\varepsilon e^{i\omega t})\frac{\partial C}{\partial y} = \frac{1}{S_c}\frac{\partial^2 C}{\partial y^2} - K_c C \tag{3.4}$$

$$\begin{aligned} &u = 0, \quad T = 1+\varepsilon e^{i\omega t}, \quad C = 1+\varepsilon e^{i\omega t}, \quad \frac{\partial^2 u}{\partial y^2} = 0, \quad \text{at } y = 0,\\ &u \to 0, \quad T \to 0, \quad C \to 0, \quad \frac{\partial^2 u}{\partial y^2} \to 0, \quad \text{as } y \to \infty. \end{aligned} \tag{3.5}$$

4. Method of Solution

Considering the effects of periodic suction, as well as the temperature and concentration near the plate, we can assume the velocity, temperature, and concentration in the vicinity of the plate are represented as follows:

$$u(y,t) = u_0(y) + \varepsilon u_1(y)e^{i\omega t} \tag{4.1}$$

$$T(y,t) = T_0(y) + \varepsilon T_1(y)e^{i\omega t} \tag{4.2}$$

$$C(y,t) = C_0(y) + \varepsilon C_1(y)e^{i\omega t} \tag{4.3}$$

Mishra et al. [9], Das et al. [3], and Gireesh Kumar and Satyanarayana [5] adopted the above form of solution to solve the periodically fluctuating flow problems.

Substituting Equations (4.1) to (4.3) into equations (3.2) to (3.4) and equating the non-harmonic (coefficient of ε^0) and harmonic (coefficient of ε) terms yields

$$-\phi\frac{d^4 u_0}{dy^4} + \frac{d^2 u_0}{dy^2} + \frac{du_0}{dy} - (M^2 + \frac{1}{K_p})u_0 = -G_r T_0 - G_c C_0 \tag{4.4}$$

$$-\phi\frac{d^4 u_1}{dy^4} + \frac{d^2 u_1}{dy^2} - (M^2 + \frac{1}{K_p} + \frac{i\omega}{4})u_1 = -\frac{du_0}{dy} - G_r T_1 - G_c C_1 - \frac{u_0}{K_p} \tag{4.5}$$

$$\frac{d^2 T_0}{dy^2} + P_r\frac{dT_0}{dy} + P_r S T_0 = 0. \tag{4.6}$$

$$\frac{d^2 T_1}{dy^2} + P_r\frac{dT_1}{dy} + P_r(S - \frac{i\omega}{4})T_1 = -P_r\frac{dT_0}{dy} \tag{4.7}$$

$$\frac{d^2 C_0}{dy^2} + S_c\frac{dC_0}{dy} - K_c S_c C_0 = 0 \tag{4.8}$$

$$\frac{d^2 C_1}{dy^2} + S_c\frac{dC_1}{dy} - \frac{i\omega}{4}S_c C_1 - K_c S_c C_1 = -S_c\frac{dC_0}{dy} \tag{4.9}$$

The boundary conditions (3.5) reduce to

$$\left.\begin{array}{l} u_0 = u_1 = 0, \quad T_0 = T_1 = 1, \quad C_0 = C_1 = 1 \quad \text{at } y = 0 \\ u_0 = u_1 \to 0, \quad T_0 = T_1 \to 0, \quad C_0 = C_1 \to 0 \quad \text{as } y \to \infty \\ \dfrac{d^2u_0}{dy^2} = 0 \quad \& \quad \dfrac{d^2u_1}{dy^2} = 0 \quad \text{at } y = 0 \\ \dfrac{d^2u_0}{dy^2} \to 0 \quad \& \quad \dfrac{d^2u_1}{dy^2} \to 0 \quad \text{as } y \to \infty \end{array}\right\} \tag{4.10}$$

The solutions of the differential equations (4.4) to (4.9) with the boundary conditions (4.10) for $u(y,t)$, $T(y,t)$, and $C(y,t)$ are obtained numerically by using the Runge-Kutta Method of order 4.

4.1 Skin-friction coefficient(τ)

The shear stress (skin friction) at the plate in terms of amplitude is given by

$$\tau = \left.\frac{\partial u_0}{\partial y}\right|_{y=0} + \varepsilon e^{i\omega t} \left.\frac{\partial u_1}{\partial y}\right|_{y=0} - \phi \left[\left.\frac{\partial^3 u_0}{\partial y^3}\right|_{y=0} + \varepsilon e^{i\omega t} \left.\frac{\partial^3 u_1}{\partial y^3}\right|_{y=0} \right]$$

4.2 Nusselt number (N_u)

The rate of heat transfer (heat flux) at the plate in terms of amplitude is given by

$$N_u = -\left[\left.\frac{\partial T_0}{\partial y}\right|_{y=0} + \varepsilon e^{i\omega t} \left.\frac{\partial T_1}{\partial y}\right|_{y=0} \right]$$

4.3 Sherwood number (S_h)

The mass transfer coefficient (The Sherwood number) at the plate in terms of amplitude is given by

$$S_h = -\left[\left.\frac{\partial C_0}{\partial y}\right|_{y=0} + \varepsilon e^{i\omega t} \left.\frac{\partial C_1}{\partial y}\right|_{y=0} \right]$$

5. Results and Discussion

The flow scenario is illustrated in Figure 2.1. It depicts convective flow of an incompressible, electrically conducting couple-stress fluid past a vertical porous plate within a porous medium with chemical reaction, and time-dependent oscillatory permeability and suction. The flow is influenced by the non-dimensional parameters Hartmann number M, Permeability Parameter K_p, Thermal Grashof number G_r, Mass Grashof number G_c, Frequency of oscillation ω, Schmidt number S_c, Prandtl number P_r, Heat source parameter S, Couple Stress parameter ϕ, Chemical reaction parameter K_c. The results of the numerical evaluation for various values of the governing parameters are shown graphically in Figure 5.1 to Figure 5.8 and Table 5.1 to Table 5.13. In the numerical work, we take $M = 1$, $\omega = 1$, $\phi = 2$, $P_r = 0.5$, $K_p = 1$, $G_c = 2$, $G_r = 2$, $S_c = 2$, $S = 3$, $\varepsilon = 1$, $t = 2$, $K_c = 1$, except where they are variables.

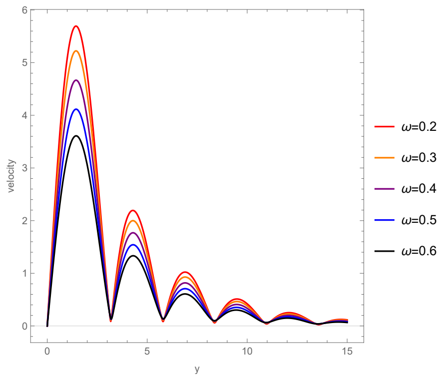

(a) Variation of u(y,t) for frequency of oscillation ω

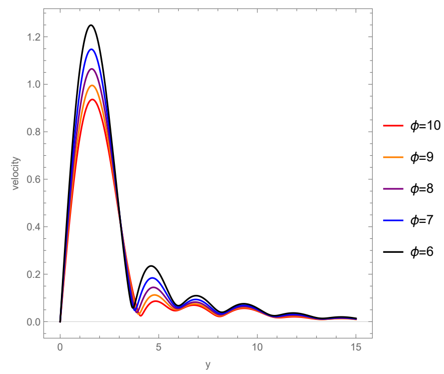

(b) Variation of u(y,t) for couple stress parameter ϕ

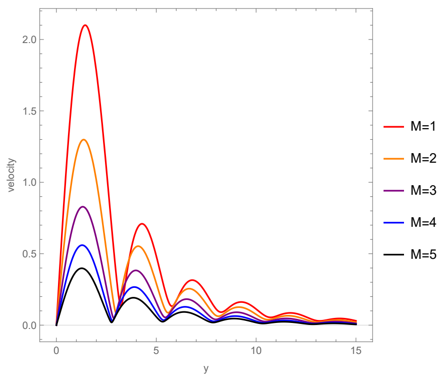

(c) Variation of u(y,t) for magnetic parameter M

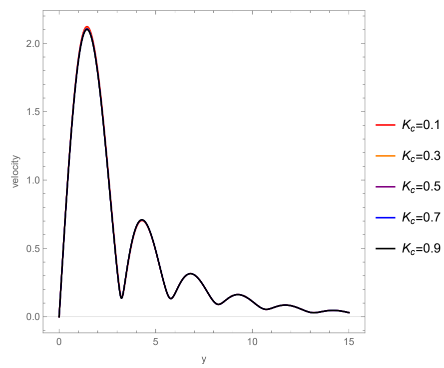

(d) Variation of $u(y,t)$ for chemical reaction parameter K_c

Figure 5.1. Variation of velocity with different flow parameters

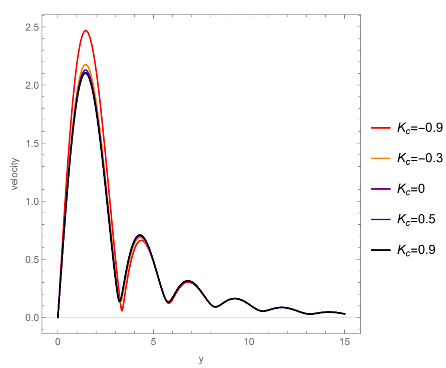

(a) Variation of $u(y,t)$ for chemical reaction parameter K_c

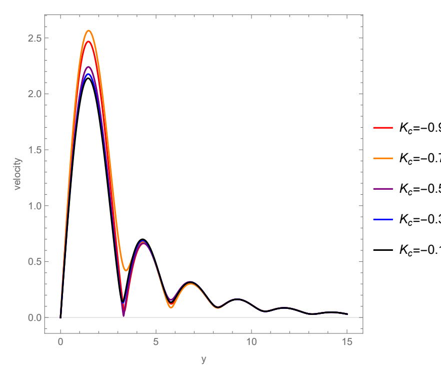

(b) Variation of $u(y,t)$ for chemical reaction parameter K_c

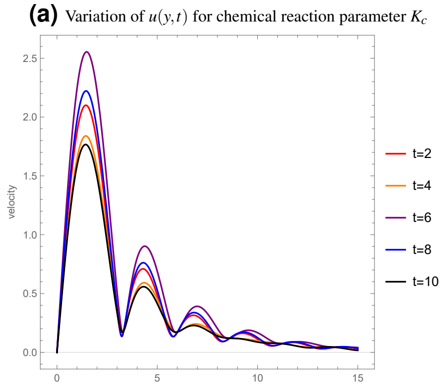

(c) Variation of u(y,t) for time t

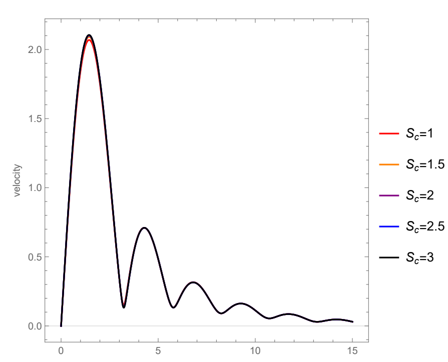

(d) Variation of $u(y,t)$ for Schmidt number S_c

Figure 5.2. Variation of velocity with different flow parameters

Figure 5.1 illustrates the variations in velocity for frequency of oscillation ω, couple-stress parameter ϕ, Hartmann number M, and chemical reaction parameter K_c . Figure 5.1a shows that an increase in the frequency of oscillation (ω) in the range 0 to 1 reduces fluid velocity. This indicates that higher oscillation frequency (in the range 0 to 1) dampens the flow. Figure 5.1b displays that an increase in the couple-stress parameter (ϕ) reduces the fluid velocity due to the internal resistance posed by couple stresses. This behavior indicates a reduction in the momentum boundary-layer thickness. An increase in the Hartmann number M (Figure 5.1c) also reduces the fluid velocity, since resulting Lorentz force opposes the fluid motion, leading to a thinner momentum boundary layer. Figures 5.1d, 5.2a, and 5.2b depict the variations of the fluid velocity with respect to chemical reaction rate (K_c). The positive value of K_c (associated with destructive reaction) reduces velocity by reducing the thickness of the boundary layer, whereas a negative value of K_c (linked to generative reaction) enhances velocity. The destructive reaction weakens species transport and consequently reduces the boundary-layer thickness. Time dependence, as depicted in Fig. 5.2c, indicates that velocity decreases over time (t), suggesting a transient slowing of the flow. This reflects the gradual stabilization of the momentum boundary layer with time. Additionally, Figure 5.2d shows that the Schmidt number (S_c) does not make a significant impact on the velocity.

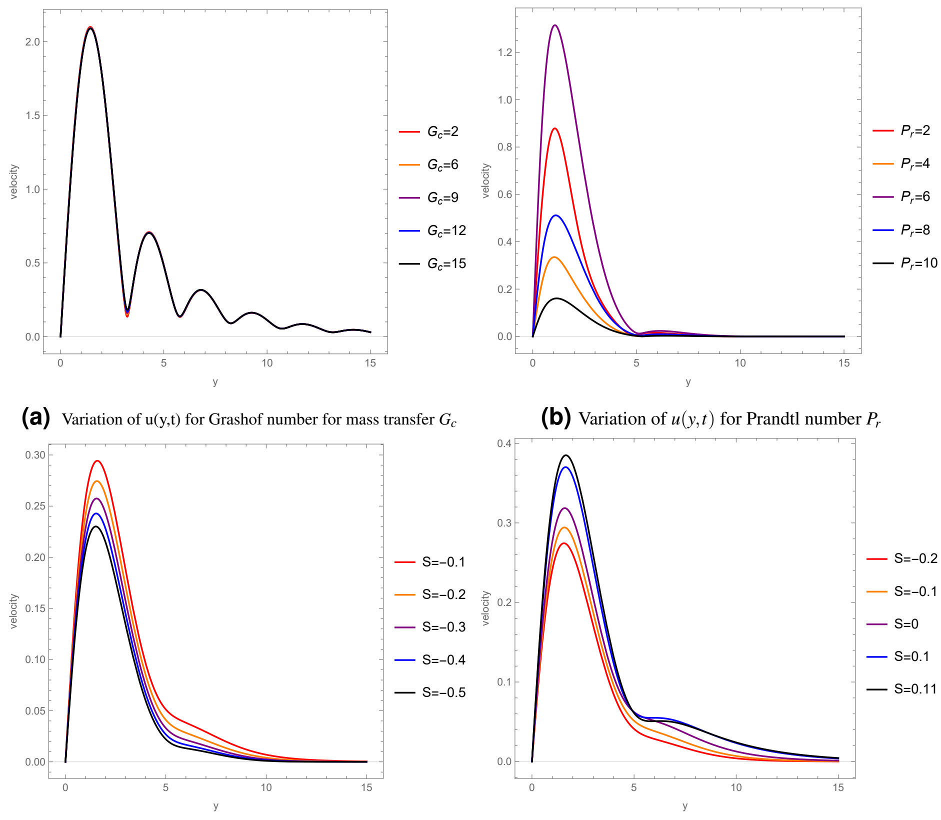

(a) Variation of u(y,t) for Grashof number for mass transfer G_c **(b)** Variation of $u(y,t)$ for Prandtl number P_r

(c) Variation of $u(y,t)$ for heat source parameter S **(d)** Variation of $u(y,t)$ for heat source parameter S

Figure 5.3. Variation of velocity with different flow parameters

Figure 5.3a demonstrates the effect of the Grashof number (G_c) (for mass transfer) on the mass transfer. The Grashof number (G_c) does not significantly impact the fluid velocity. Figure 5.3b shows that higher Prandtl numbers (P_r) reduce the fluid velocity due to lower thermal diffusivity. The effects of the heat source parameter (S) on the velocity are depicted in Figures 5.3c, 5.3d, and 5.4a. Figure 5.3c illustrates that the negative heat source parameter decreases the fluid velocity, behaving as a heat sink. Figure 5.3d shows that the positive heat source parameter behaves as a heat source, increasing the velocity, whereas the negative heat source parameter behaves as a heat sink, decreasing the velocity. When S is high, then the fluid velocity decreases with S due to the stabilising effect. The added thermal energy thickens the thermal boundary layer and enhances buoyancy effects. The removal of thermal energy causes the thermal boundary layer to become thinner. Figure 5.4b indicates that as ε increases, the velocity increases. Figure 5.4c shows that the Grashof number (G_r) (for heat transfer) increases the velocity due to a greater buoyancy force, which leads to increase in the momentum boundary-layer thickness. The permeability parameter (K_p) also increases velocity (Figure 5.4d) because the porous medium offers less resistance to the flow. The reduction in porous-medium resistance promotes the growth of the momentum boundary layer.

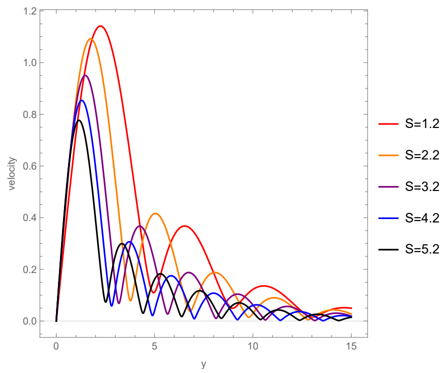

(a) Variation of $u(y,t)$ for heat source parameter S

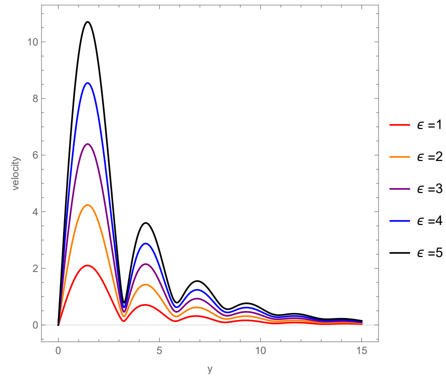

(b) Variation of $u(y,t)$ for positive Constant ε

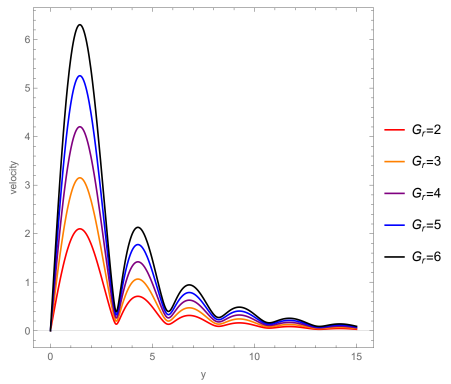

(c) Variation of $u(y,t)$ for Grashof number for heat transfer G_r

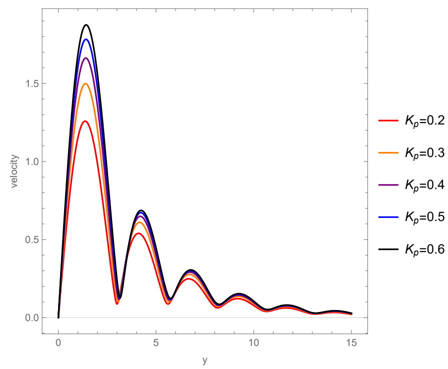

(d) Variation of $u(y,t)$ for permeability parameter K_p

Figure 5.4. Variation of velocity with different flow parameters

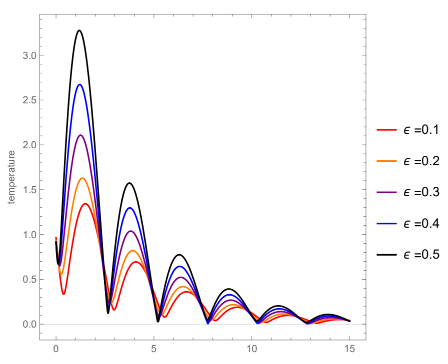

(a) Variation of T(y,t) for positive constant ε

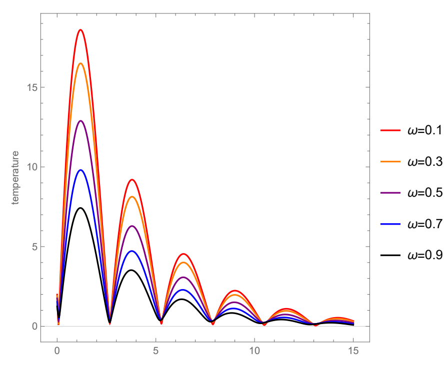

(b) Variation of T(y,t) for frequency of oscillation ω

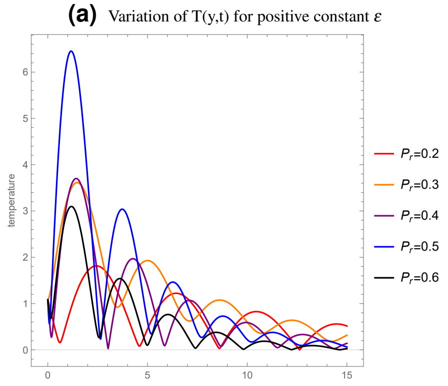

(c) Variation of T(y,t) for Prandtl number P_r

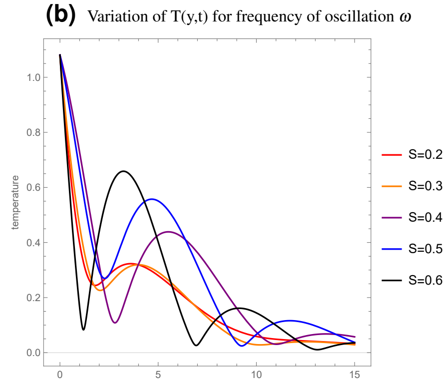

(d) Variation of T(y,t) for heat source parameter S

Figure 5.5. Variation of temperature with different flow parameters

Figures 5.5 and 5.6 highlight the influence of different flow parameters on the temperature profiles. Figure 5.5a shows that an increase in the positive constant (ε) leads to an increase in the temperature, whereas Figure 5.5b illustrates that an increase in the frequency of oscillation (ω) decreases the temperature. The influence of the Prandtl number (P_r), as depicted in Figure 5.5c, demonstrates that higher values of (P_r) lead to a decrease in temperature. This is due to reduced heat diffusion compared to momentum, which results in a thinner thermal boundary layer. Figures 5.5d, 5.6a, 5.6b present the effects of heat source parameter (S) on the temperature profiles. An increase in the positive heat source parameter leads to a rise in the temperature due to internal heat generation, whereas an increase in the negative heat source parameter causes a decrease in the temperature. Figure 5.6c depicts that temperature shows oscillatory behavior with time (t) due to time-dependent permeability and suction velocity.

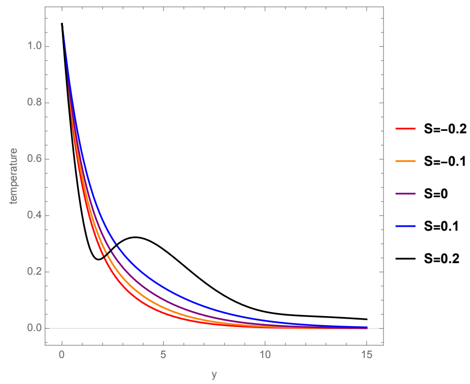

(a) Variation of T(y,t) for heat source parameter S

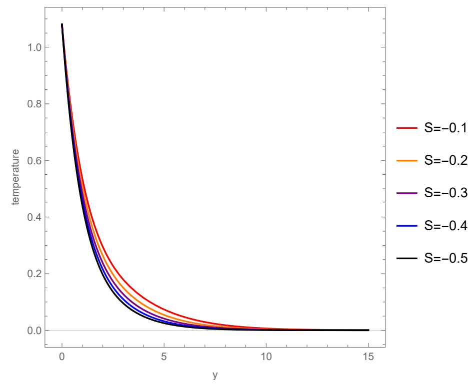

(b) Variation of T(y,t) for heat source parameter S

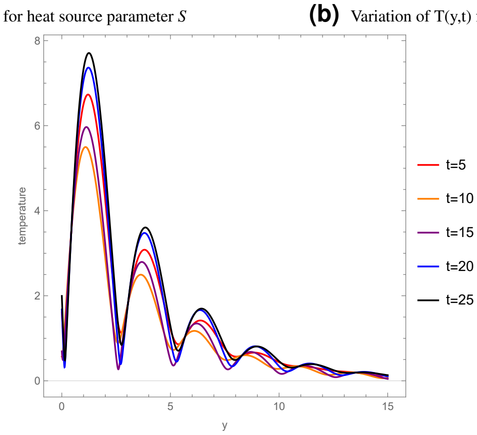

(c) Variation of T(y,t) for time t

Figure 5.6. Variation of temperature with different flow parameters

Figures 5.7 and 5.8 present the effects of various flow parameters on the concentration distribution. Figures 5.7a, 5.7b, and 5.7c show that for positive values of (K_c), which indicates a destructive chemical reaction, increasing K_c leads to a decrease in concentration as the chemical reaction consumes the diffusing species. For negative values of K_c, which indicate a generative reaction, a higher magnitude of K_c enhances concentration. Figure 5.7d depicts that an increase in the positive constant ε decreases concentration, while Figure 5.8a shows that a higher frequency of oscillation ω increases the concentration. The Schmidt number (S_c), as depicted in Figure 5.8b, demonstrates that an increase in S_c decreases the concentration due to reduced mass diffusivity, which leads to a thinner concentration boundary layer. Figure 5.8c reveals that concentration increases with time t. Figures 5.9a and 5.9b are depicted for the limiting case of $\phi = 0$ (absence of couple-stress effects). The velocity profiles are similar to that reported by Das et al. [3], thereby confirming the reliability of the present formulation and numerical implementation.

The variations in shear stress (τ), Nusselt number (N_u), and Sherwood number (S_h) with respect to various flow parameters are presented numerically in Tables 5.1-5.13.

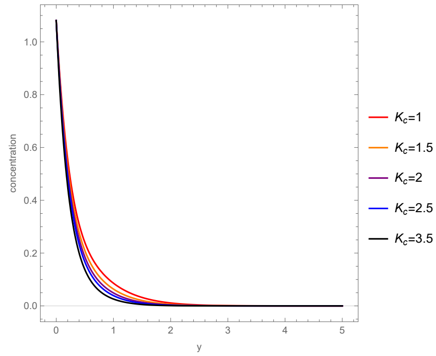

(a) Variation of C(y,t) for chemical reaction parameter K_c

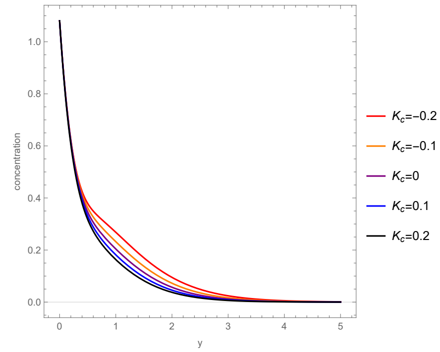

(b) Variation of C(y,t) for chemical reaction parameter K_c

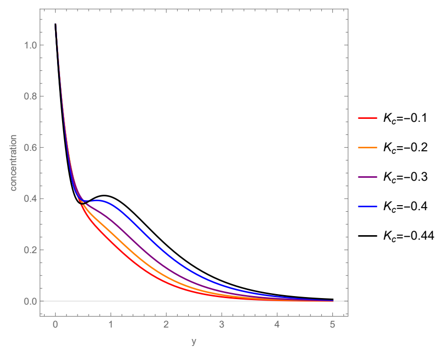

(c) Variation of C(y,t) for chemical reaction parameter K_c

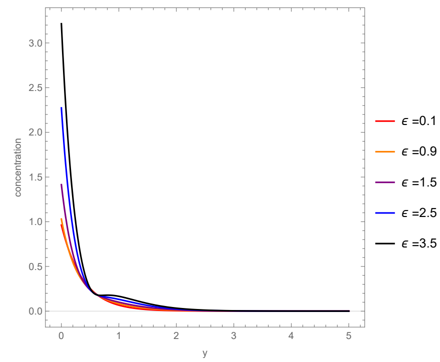

(d) Variation of C(y,t) for a small positive constant ε

Figure 5.7. Variation of concentration with different flow parameters

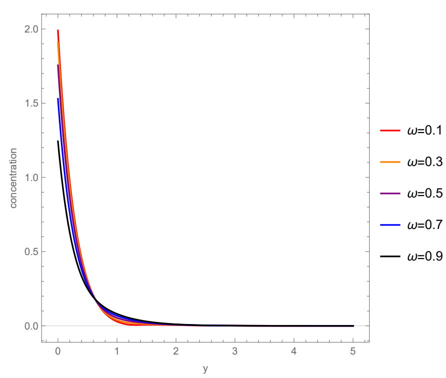

(a) Variation of C(y,t) for frequency of oscillation ω

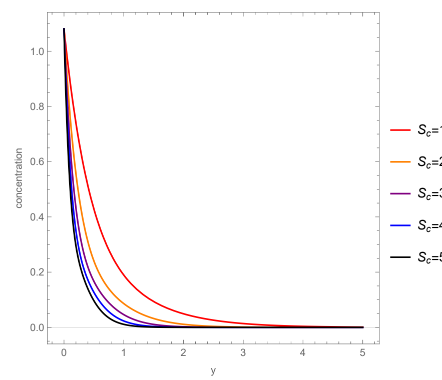

(b) Variation of C(y,t) for Schmidt number S_c

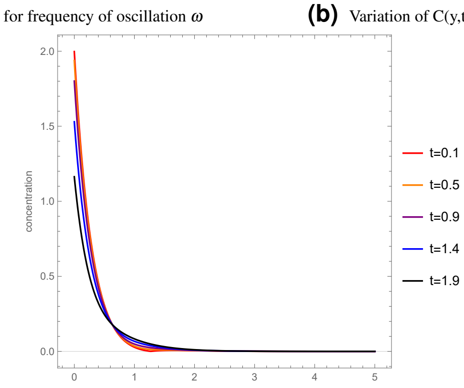

(c) Variation of C(y,t) for time t

Figure 5.8. Variation of concentration with different flow parameters

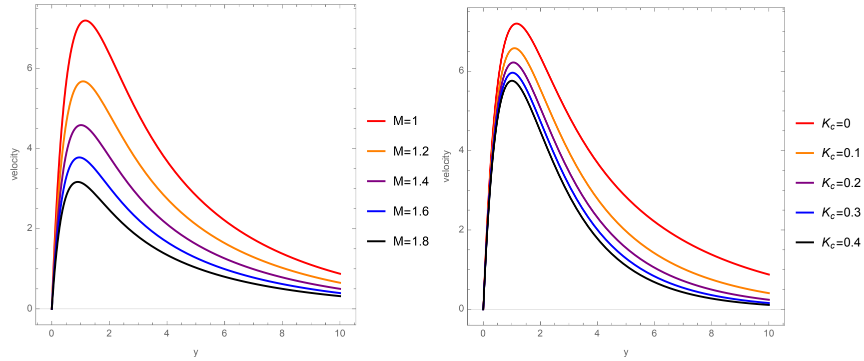

(a) Variation of u(y,t) for M **(b)** Variation of u(y,t) for K_c

Figure 5.9. Variation of velocity with different flow parameters for $\phi = 0$

Table 5.1 shows the variation in shear stress with respect to the Hartmann number M. As the M increases from 0 to 4, the shear stress at the plate consistently decreases. The Table 5.2 presents the effect of the couple-stress parameter ϕ on shear stress at the plate. As ϕ decreases from 10 to 6, the shear stress at the plate increases. The data in the Table 5.3 indicates that as the permeability parameter K_p increases from 0.2 to 0.6, the shear stress at the plate also increases. The Table 5.4 presents the variations in shear stress with the Prandtl number P_r. The values show a mixed trend with P_r. The Table 5.5 shows that as the Grashof number for mass transfer G_c increases from 2 to 15, the shear stress at the plate decreases for $\omega t = 0, \frac{\pi}{4}, \frac{\pi}{2}$, whereas the shear stress at the plate increases for $\omega t = \frac{3\pi}{4}$. The Table 5.6 shows that as the Grashof number for heat transfer G_r increases from 2 to 6, the shear stress at the plate also increases. The Table 5.7 presents the variations with respect to the Schmidt number S_c. As the Schmidt number S_c increases from 1 to 3, the shear stress at the plate also increases. The Table 5.8 represents that as the heat source parameter S increases from 1.2 to 5.2, the shear stress decreases for $\omega t = 0$. For $\omega t = \frac{\pi}{4}$, shear stress increases with increase in S from 1.2 to 2.2, and further increase in S leads to decrease in the shear stress. The shear stress increases with an increase in S for $\omega t = \frac{\pi}{2}, \frac{3\pi}{4}$. The Table 5.9 illustrates the effects of the chemical reaction parameter K_c on the shear stress. As K_c increases from -0.9 to 0.9, the shear stress at the plate decreases. Variations in the Nusselt number with respect to the Prandtl number P_r are presented in Table 5.10. It is observed that there is no change in the shear stress for $\omega t = 0$, while for $\omega t = \frac{\pi}{4}, \frac{\pi}{2}, \frac{3\pi}{4}$, the shear stress increases then decreases with an increase in the Prandtl number. The Table 5.11 shows the variations in the Nusselt number with the heat source parameter S . At $\omega t = 0$, the Nusselt number remains constant for all values of S. However, for $\omega t = \frac{\pi}{4}, \frac{\pi}{2}$, the Nusselt number increases with S. For $\omega t = \frac{3\pi}{4}$, the Nusselt number shows mixed trends with S. The Table 5.12 presents the variations in the Sherwood number with the Schmidt number S_c. As S_c increases from 1 to 5, the Sherwood number consistently increases. The Table 5.13 shows the effects of the chemical reaction parameter K_c on the Sherwood number. As K_c increases from -0.2 to 0.2, the Sherwood number increases at $\omega t = 0, \frac{\pi}{4}, \frac{\pi}{2}$, whereas the Sherwood number decreases at $\omega t = \frac{3\pi}{4}$.

ωt	$M = 0$	$M = 1$	$M = 2$	$M = 3$	$M = 4$
0	7.84927	6.23203	4.10145	2.71176	1.86848
$\frac{\pi}{4}$	6.58473	5.2168	3.42372	2.25924	1.55433
$\frac{\pi}{2}$	3.95976	3.11081	2.02415	1.33014	0.913112
$\frac{3\pi}{4}$	2.35311	1.83255	1.18986	0.787435	0.545948

Table 5.1. Variation in Shear Stress at the Plate with Magnetic Parameter M at ϕ = 2, K_p = 1, P_r = 0.5, G_c = 2, G_r = 2, S_c = 2, S = 3, ε = 1 , K_c = 1.

ωt	$\phi = 10$	$\phi = 9$	$\phi = 8$	$\phi = 7$	$\phi = 6$
0	2.47823	2.65871	2.87246	3.12975	3.44678
$\frac{\pi}{4}$	2.07828	2.22952	2.37934	2.62345	2.89082
$\frac{\pi}{2}$	1.24458	1.33246	1.43872	1.56813	1.7241
$\frac{3\pi}{4}$	0.721694	0.774502	0.836586	0.909311	1.00431

Table 5.2. Variation in Shear Stress at the Plate with Couple Stress Parameter ϕ at M = 1, ω = 1, K_p = 1, P_r = 0.5, G_c = 2, G_r = 2, S_c = 2, S = 3, ε = 1, t = 2 , $K_c = 1$.

ωt	$K_p = 0.2$	$K_p = 0.3$	$K_p = 0.4$	$K_p = 0.5$	$K_p = 0.6$
0	3.8112	4.51099	4.98469	5.32967	5.59343
$\frac{\pi}{4}$	3.19369	3.77954	4.17568	4.46394	4.68417
$\frac{\pi}{2}$	1.924	2.27094	2.50409	2.67298	2.80156
$\frac{3\pi}{4}$	1.17142	1.36919	1.50003	1.59377	1.66453

Table 5.3. Variation in Shear Stress at the Plate with Permeability Parameter K_p at M = 1, ϕ = 2, P_r = 0.5, G_c = 2, G_r = 2, S_c = 2, S = 3, ε = 1, $K_c = 1$.

ωt	$P_r = 0.5$	$P_r = 0.6$	$P_r = 0.7$	$P_r = 0.8$	$P_r = 0.9$
0	3.38698	1.42762	2.0916	1.37594	1.55603
$\frac{\pi}{4}$	3.34359	1.33834	1.92532	1.29835	1.56905
$\frac{\pi}{2}$	3.11081	1.28499	1.76729	1.25182	1.53364
$\frac{3\pi}{4}$	2.8008	1.30394	1.72221	1.26757	1.46832

Table 5.4. Variation in Shear Stress at the Plate with Prandtl Number P_r at M = 1, ϕ = 2, K_p = 1, G_c = 2, G_r = 2, S_c = 2, S = 3, ε = 1 , $K_c = 1$.

ωt	$G_c = 2$	$G_c = 6$	$G_c = 9$	$G_c = 12$	$G_c = 15$
0	6.23203	6.10512	6.00994	5.91476	5.81958
$\frac{\pi}{4}$	5.2168	5.10449	5.02051	4.93673	4.85322
$\frac{\pi}{2}$	3.11081	3.05098	3.00765	2.96568	2.92516
$\frac{3\pi}{4}$	1.83255	1.84596	1.85832	1.87263	1.88882

Table 5.5. Variation in Shear Stress at the Plate with Grashof Number for Mass Transfer G_c at M = 1, ϕ = 2, K_p = 1, P_r = 0.5, G_r = 2, S_c = 2, S = 3, ε = 1, $K_c = 1$.

ωt	$G_r = 2$	$G_r = 3$	$G_r = 4$	$G_r = 5$	$G_r = 6$
0	6.23203	9.37978	12.5275	15.6753	18.823
$\frac{\pi}{4}$	5.2168	7.85331	10.4899	13.1264	15.763
$\frac{\pi}{2}$	3.11081	4.68152	6.25226	7.823	9.39374
$\frac{3\pi}{4}$	1.83255	2.74599	3.65951	4.57306	5.48661

Table 5.6. Variation in Shear Stress at the Plate with Grashof Number for Heat Transfer G_r at $M = 1$, $\phi = 2$, $K_p = 1$, $P_r = 0.5$, $G_c = 2$, $S_c = 2$, $S = 3$, $\varepsilon = 1$, $K_c = 1$.

ωt	$S_c = 1$	$S_c = 1.5$	$S_c = 2$	$S_c = 2.5$	$S_c = 3$
0	6.12746	6.19717	6.23203	6.25179	6.26395
$\frac{\pi}{4}$	5.1209	5.18497	5.2168	5.23469	5.24566
$\frac{\pi}{2}$	3.04385	3.08922	3.11081	3.12242	3.12919
$\frac{3\pi}{4}$	1.80557	1.82516	1.83255	1.83536	1.83625

Table 5.7. Variation in Shear Stress at the Plate with Schmidt Number S_c at $M = 1$, $\phi = 2$, $K_p = 1$, $P_r = 0.5$, $G_c = 2$, $G_r = 2$, $S = 3$, $\varepsilon = 1$, $K_c = 1$.

ωt	$S = 1.2$	$S = 2.2$	$S = 3.2$	$S = 4.2$	$S = 5.2$
0	3.33238	1.83479	1.23526	1.01992	0.838607
$\frac{\pi}{4}$	2.21014	2.34165	2.11894	1.92829	1.99953
$\frac{\pi}{2}$	1.02698	1.27028	1.29547	1.30924	1.36139
$\frac{3\pi}{4}$	0.612266	0.785562	0.829047	0.860343	0.896516

Table 5.8. Variation in Shear Stress at the Plate with Heat Source Parameter S at $M = 1$, $\phi = 2$, $K_p = 1$, $P_r = 0.5$, $G_c = 2$, $G_r = 2$, $S_c = 2$, $\varepsilon = 1$, $K_c = 1$.

ωt	$K_c = -0.9$	$K_c = -0.3$	$K_c = 0$	$K_c = 0.5$	$K_c = 0.9$
0	18.6898	6.27508	6.23249	6.22809	6.23113
$\frac{\pi}{4}$	7.22339	5.26278	5.22083	5.21416	5.21611
$\frac{\pi}{2}$	3.63583	3.17271	3.12878	3.11332	3.11098
$\frac{3\pi}{4}$	2.16287	1.9192	1.8698	1.84234	1.83392

Table 5.9. Variation in Shear Stress at the Plate with chemical reaction parameter K_c at $M = 1$, $\phi = 2$, $K_p = 1$, $P_r = 0.5$, $G_c = 2$, $G_r = 2$, $S_c = 2$, $\varepsilon = 1$, $S = 3$.

ωt	$P_r = 0.2$	$P_r = 0.3$	$P_r = 0.4$	$P_r = 0.5$	$P_r = 0.6$
0	7.04145	7.04145	7.04145	7.04145	7.04145
$\frac{\pi}{4}$	2.74885	10.0394	11.781	25.7478	14.08
$\frac{\pi}{2}$	2.18377	6.10766	7.66949	15.5582	7.83177
$\frac{3\pi}{4}$	1.40711	3.35268	4.66545	9.18175	4.83748

Table 5.10. Variation in Nusselt Number at the Plate with Prandtl Number P_r at M = 1, ϕ = 2, K_p = 1, G_c = 2, G_r = 2, S_c = 2, S = 3, ε = 1, $K_c = 1$.

ωt	$S = 0.2$	$S = 0.3$	$S = 0.4$	$S = 0.5$	$S = 0.6$
0	7.04145	7.04145	7.04145	7.04145	7.04145
$\frac{\pi}{4}$	1.24586	1.82303	2.17996	2.71561	2.76007
$\frac{\pi}{2}$	1.39188	1.12359	0.553382	0.798491	1.4302
$\frac{3\pi}{4}$	0.811645	0.707379	0.279505	0.319558	0.863866

Table 5.11. Variation in Nusselt Number at the Plate with Heat Source Parameter S at M = 1, ϕ = 2, K_p = 1, P_r = 0.5, G_c = 2, G_r = 2, S_c = 2, ε = 1, $K_c = 1$.

ωt	$S_c = 1$	$S_c = 2$	$S_c = 3$	$S_c = 4$	$S_c = 5$
0	3.95967	7.04145	10.0646	13.0711	16.0716
$\frac{\pi}{4}$	3.65987	6.52441	9.33834	12.1387	14.9345
$\frac{\pi}{2}$	2.81398	5.06993	7.29933	9.52439	11.7495
$\frac{3\pi}{4}$	1.59814	3.00646	4.42951	5.86487	7.30889

Table 5.12. Variation in Sherwood Number at the Plate with Schmidt Number S_c at M = 1, ϕ = 2, K_p = 1, P_r = 0.5, G_c = 2, G_r = 2, S = 3, ε = 1, $K_c = 1$.

ωt	$K_c = -0.2$	$K_c = -0.1$	$K_c = 0$	$K_c = 0.1$	$K_c = 0.2$
0	5.84019	5.90689	6.00000	6.10376	6.21159
$\frac{\pi}{4}$	5.46089	5.51301	5.59113	5.68081	5.77558
$\frac{\pi}{2}$	4.41239	4.42013	4.45393	4.50215	4.55848
$\frac{3\pi}{4}$	3.00717	2.94423	2.90765	2.8891	2.88291

Table 5.13. Variation in Sherwood Number at the Plate with chemical reaction parameter K_c at M = 1, ϕ = 2, K_p = 1, P_r = 0.5, G_c = 2, G_r = 2, S = 3, ε = 1, S_c = 2 .

6. Conclusions

The analysis presented provides the following results of physical interest regarding the velocity, temperature and concentration distribution of the flow field, as well as skin friction, the Nusselt number, and the Sherwood number. In the study, the plate is considered infinite, radiation is negligible, and Soret-Dufour effects are neglected. The future scope of this study is to explore the combined effect of different flow parameters, the effect of radiation, non-linear reactions, or fractional order modeling.

- The velocity of the couple-stress fluid decreases as the Hartmann number (M), the frequency of oscillation (ω), the couple-stress parameter (ϕ), and the positive chemical reaction parameter (K_c) increase. The resistive effects, such as the Lorentz force, internal couple stresses, and destructive reactions, cause this.
- The velocity increases with an increase in Grashof number for heat transfer (G_r), permeability parameter (K_p), and oscillatory suction parameter (ε), due to stronger buoyancy and permeability effects.
- The Prandtl number (P_r) affects both velocity and temperature. An increase in P_r results in lower thermal diffusivity, leading to a thinner thermal boundary layer and reduced heat transfer.
- The Schmidt number (S_c) decreases concentration and velocity due to reduced mass diffusivity, which results in a thinner concentration boundary layer.
- The heat source parameter (S) has a dual effect: a positive S enhances temperature and velocity through internal heat generation. A negative S (acting as a heat sink) decreases the temperature and the velocity.
- Positive values of chemical reaction parameter (K_c) (destructive reactions) reduce velocity and concentration by consuming diffusing species, whereas negative values (generative reactions) enhance both velocity and concentration
- The shear stress at the plate decreases with an increase in M and K_c, but increases with an increase in K_p, G_r, and S_c.
- The Nusselt number (N_u) shows mixed trends to P_r and S, generally increasing with greater S under oscillatory conditions, and remains constant at $\omega t = 0$.
- The Sherwood number (S_h) increases with both S_c and K_c, indicating enhanced mass transfer under conditions of higher diffusivity and generative reactions.

Article Information

Acknowledgements: The authors would like to express their sincere thanks to the editor and the anonymous reviewers for their helpful comments and suggestions.

Author Contributions: Conceptualization: DK, MKM; Methodology: DK, MKM; Software: DK, MKM; Validation: DK, MKM; Formal analysis: DK, MKM; Investigation: DK, MKM; Resources: DK, MKM; Writing – original draft: DK, MKM; Writing – review & editing: DK; Visualization: DK, MKM;

Artificial Intelligence Statement: The authors declare that no artificial intelligence tools were used in the conceptualization, analysis, writing or interpretation of this manuscript, except for minor grammar correction.

Conflict of Interest Disclosure: No potential conflict of interest was declared by authors.

Plagiarism Statement: This article was scanned by the plagiarism program.

References

[1] A. J. Chamkha, *Unsteady MHD convective heat and mass transfer past a semi-infinite vertical permeable moving plate with heat absorption*, Internat. J. Engrg. Sci., **42**(2) (2004), 217–230. https://doi.org/10.1016/S0020-7225(03)00285-4

[2] R. V. Prasad, B. N. Reddy, *Radiation and mass transfer effects on an unsteady MHD free convection flow past a heated vertical plate in a porous medium with viscous dissipation*, Theor. Appl. Mech., **34**(2) (2007), 135–160. https://doi.org/10.2298/TAM0702135P

[3] S. S. Das, A. Satapathy, J. K. Das, et al., *Mass transfer effects on MHD flow and heat transfer past a vertical porous plate through a porous medium under oscillatory suction and heat source*, Int. J. Heat Mass Transf., **52**(25-26) (2009), 5962–5969. https://doi.org/10.1016/j.ijheatmasstransfer.2009.04.038

[4] P. Ram, A. Kumar, H. Singh, *The effect of chemical reaction and heat transfer on MHD flow of viscous fluid past a moving isothermal vertical porous plate with time-dependent suction*, Int. J. Theor. Appl. Mech., **6**(3) (2011), 241–254.

[5] J. G. Kumar, P. V. Satyanarayana, *Mass transfer effect on MHD unsteady free convective Walter's memory flow with constant suction and heat sink*, Int. J. Appl. Math. Mech., **7**(19) (2011), 97–109.

[6] J. A. Rao, S. Sivaiah, R. S. Raju, *Chemical reaction effects on an unsteady MHD free convection fluid flow past a semi-infinite vertical plate embedded in a porous medium with heat absorption*, J. Appl. Fluid Mech., **5**(3) (2012), 63–72. https://doi.org/10.36884/jafm.5.03.19446

[7] S. Shivaiah, A. J. Rao, *Chemical reaction effect on an unsteady MHD free convection flow past a vertical porous plate in the presence of suction or injection*, Theor. Appl. Mech., **39**(2) (2012), 185–208.

[8] K. Sarada, B. Shanker, *The effect of chemical reaction on an unsteady MHD free convection flow past an infinite vertical porous plate with variable suction*, Int. J. Mod. Eng. Res., **3**(2) (2013), 725–735.

[9] S. R. Mishra, G. C. Dash, M. Acharya, *Mass and heat transfer effect on MHD flow of a visco-elastic fluid through porous medium with oscillatory suction and heat source*, Int. J. Heat Mass Transf., **57**(2) (2013), 433–438. https://doi.org/10.1016/j.ijheatmasstransfer.2012.10.053

[10] N. A. Khan, F. Riaz, F. Sultan, *Effects of chemical reaction and magnetic field on a couple stress fluid over a non-linearly stretching sheet*, Eur. Phys. J. Plus, **129**(1) (2014), Article ID 18. https://doi.org/10.1140/epjp/i2014-14018-2

[11] M. K. Nayak, G. C. Dash, L. P. Singh, *Effect of chemical reaction on MHD flow of a visco-elastic fluid through porous medium*, J. Appl. Anal. Comput., **4**(4) (2014), 367–381. https://doi.org/10.11948/2014020

[12] K. S. Balamurugan, J. L. Ramaprasad, S. V. K. Varma, *Unsteady MHD free convective flow past a moving vertical plate with time dependent suction and chemical reaction in a slip flow regime*, Procedia Eng., **127** (2015), 516–523. https://doi.org/10.1016/j.proeng.2015.11.338

[13] P. K. Rout, S. N. Sahoo, G. C. Dash, et al., *Chemical reaction effect on MHD free convection flow in a micropolar fluid*, Alex. Eng. J., **55**(3) (2016), 2967–2973. https://doi.org/10.1016/j.aej.2016.04.033

[14] K. R. Babu, A. Parandhama, K. V. Raju, et al., *Unsteady MHD free convective flow of a visco-elastic fluid past an infinite vertical porous moving plate with variable temperature and concentration*, Int. J. Appl. Comput. Math., **3**(4) (2017), 3411–3431. https://doi.org/10.1007/s40819-017-0306-8

[15] E. Kumaresan, A. G. Vijaya Kumar, J. Prakash, *Exact solution of unsteady MHD free convective chemically reacting visco-elastic fluid flow past a moving vertical plate through porous medium*, Int. J. Appl. Comput. Math., **3**(4) (2017), 3897–3923. https://doi.org/10.1007/s40819-017-0327-3

[16] K. Raghunath, R. S. Prasad, G. S. S. Raju, *Heat and mass transfer on MHD flow of non-Newtonian fluid over an infinite vertical porous plate*, Int. J. Appl. Eng. Res., **13** (2018), 11156–11163.

[17] R. Choudhury, B. Dey, *Unsteady thermal radiation effects on MHD convective slip flow of visco-elastic fluid past a porous plate embedded in porous medium*, Int. J. Appl. Math. Stat., **57**(2) (2018), 215–226.

[18] S. S. Kumari, G. S. S. Raju, *Unsteady MHD free convective flow past a vertical porous plate with span-wise fluctuating heat and mass transfer effects*, Fluid Dyn. Mater. Process., **15**(5) (2019), 471–489. https://doi.org/10.32604/fdmp.2019.04222

[19] M. Arif, P. Kumam, W. Kumam, et al., *Analysis of newly developed fractal-fractional derivative with power law kernel for MHD couple stress fluid in channel embedded in a porous medium*, Sci. Rep., **11** (2021), Article ID 20858. https://doi.org/10.1038/s41598-021-00163-3

[20] M. Waseem, T. Gul, I. Khan, et al., *Gravity-driven hydromagnetic flow of couple stress hybrid nanofluid with homogenous-heterogeneous reactions*, Sci. Rep., **11** (2021), Article ID 17498. https://doi.org/10.1038/s41598-021-97045-5

[21] O. Mopuri, C. Ganteda, B. Mahanta, et al., *MHD heat and mass transfer steady flow of a convective fluid through a porous plate in the presence of multiple parameters*, J. Adv. Res. Fluid Mech. Therm. Sci., **89**(2) (2022), 56–75. https://doi.org/10.37934/arfmts.89.2.5675

[22] S. Ravikumar, M. Rafiq, D. Abduvalieva, et al., *Effects of Joule heating and reaction mechanisms on couple stress fluid flow with peristalsis in the presence of a porous material through an inclined channel*, Open Phys., **21** (2023), Article ID 20230118. https://doi.org/10.1515/phys-2023-0118

[23] S. Sharma, S. Jain, *Chemical reactions on MHD couple stress fluids towards stretchable inclined cylinder*, J. Heat Mass Transf. Res., **11**(1) (2024), 139–150. https://doi.org/10.22075/JHMTR.2024.31241.1463

[24] R. Kavitha, J. Angel, *Impact of rotation and chemical reactions on MHD mixed convection flow over an inclined heated porous plate with heat and mass transfer analysis*, WSEAS Trans. Fluid Mech., **20** (2025), 40–50. https://doi.org/10.37394/232013.2025.20.5

Appendix

Nomenclature

C'	Species concentration	D	Molecular diffusivity
G_r	Grashof number for heat transfer	K_p	Permeability Parameter
α	Thermal diffusivity	K'_p	Permeability of the medium
S	Heat source parameter	T	Non-dimensional temperature
t	Non-dimensional time	u	Non-dimensional velocity
v_0	Constant suction velocity	y	Non-dimensional distance along y-axis
ε	A small positive constant	β'	Volumetric coefficient of expansion with species concentration
β	Volumetric coefficient of expansion for heat transfer	$\nu = \frac{\mu}{\rho}$	Kinematic coefficient of viscosity
σ	Electrical conductivity	ω	Non-dimensional frequency of oscillation
C	Non-dimensional species concentration	G_c	Grashof number for mass transfer
g	Acceleration due to gravity	K_c	Chemical reaction parameter
M	Magnetic parameter	B_0	Magnetic field of uniform strength
P_r	Prandtl number	S_c	Schmidt number
T'	Temperature of the fluid	t'	Time
u'	Velocity component along x-axis	$v(t')$	Suction velocity
y'	Distance along y-axis	ρ	Density of the fluid
ω'	Frequency of oscillation	w	Condition on porous plate
τ	Skin friction	ϕ	Non-dimensional couple stress parameter
η	Couple stress coefficient	N_u	Nusselt Number
S_h	Sherwood Number	μ	viscosity

Communications in Advanced Mathematical Sciences
ISSN (Online) 2651-4001
Vol. 9, No. 2, 77-91, 2026
https://doi.org/10.33434/cams.1903798
Research Article

Jacobsthal Trees and Generalized $\kappa x \pm 1$ Transformations

Petro Kosobutskyy[1], David Mailland[2]*

Abstract

We introduce a structural framework for the study of generalized $\kappa x \pm 1$ transformations on the set of natural numbers. The approach is based on generalized Jacobsthal sequences, which generate a family of branching structures called Jacobsthal trees.
Within this framework, classical Collatz-type iterations appear as reverse trajectories along the branches of these trees. We establish periodicity properties of the node structure, derive recurrence relations governing the formation of branching nodes, and prove structural identities linking consecutive periods.
These results provide a structural reformulation of $\kappa x \pm 1$ discrete dynamical systems in terms of Jacobsthal-type constructions.
The proposed representation reveals intrinsic periodic symmetries and partition properties of the set $\mathbb{N}$ that are not explicit in the standard iterative formulation.

Keywords: Generalized $\kappa x \pm 1$ transformations, Jacobsthal sequences, Discrete dynamical systems, Recurrence relations, Number-theoretic trees

[1] *Institute of Computer Science and Information Technologies, Lviv Polytechnic National University, Lviv, Ukraine, petkosob@gmail.com*
[2] *Independent Researcher, david.mailland@protonmail.com*
***Corresponding author**

Received: 5 March 2026, **Accepted:** 2 June 2026, **Available online:** 12 June 2026
How to cite this article: P. Kosobutskyy, D. Mailland, *Jacobsthal trees and generalized $\kappa x \pm 1$ transformations*, Commun. Adv. Math. Sci., 9(2) (2026), 77-91.

1. Introduction

1.1 Brief introduction and motivation

The classical Collatz problem is based on two arithmetic operations on numbers from the set $\mathbb{N}$ of natural numbers:

- Division by 2 of an even integer q_E until an odd value is reached.
- Transformation of an odd integer q_O into an even one by the Collatz function

$$C_{3q}^{+} = 3q_O + 1.$$

Thus, the corresponding Collatz sequences $CS_{3,q}^{+}$ are conjectured to eventually reach 1 for all initial values, a property verified for numbers up to 2^{71} [1]. This naturally suggests that the classical Collatz problem admits natural generalizations. Accordingly, the aim of this work is not to prove the classical Collatz conjecture, but to develop a generalized structural framework for $\kappa x \pm 1$ transformations based on Jacobsthal-type trees. Related studies on recurrence structures and transformations associated with generalized integer sequences include investigations on k-Narayana sequences and their binomial transforms [2], as well as works on binomial transforms of k-Jacobsthal sequences [3]. Related structural studies on generalized recursive sequence spaces were investigated in [4]. Structural approaches based on directed graph representations and acyclic graph topology were also investigated in [5]. Alternative structural and certificate-based approaches to the $3x+1$ problem have also been proposed in recent studies on finite-certificate and 2-adic formulations [6].

In 2024, Nathanson [7] studied permutation patterns of the iterated Syracuse function (a normalised form of the classical $3x+1$ map) and discussed its structure. Our paper extends this line of research to the general family of transformations $(1,3,5,7,\dots)\cdot q \pm 1$.

The aim of this work is to establish common regularities of number transformations in the general case of the transformation function $(1,3,5,7,\dots)\cdot q \pm 1$ for odd $q \in \mathbb{N}$, on the basis of which we investigate the proposed model of partitioning the set $\mathbb{N}$ into non-intersecting, isolated subsets belonging to trees of graphs with individual root sequences. As a first step, this model was originally developed by the authors [8] for the classical problem $C^{\pm}_{3,q} = 3q \pm 1$.

Here, from the perspective of transforming an odd number, mirror transformations are equivalent in structure. Indeed, since $q \in \mathbb{N}$ is odd, let $Q = -q \in \mathbb{Z}$. Then

$$3Q+1 = -3q+1 = -(3q-1).$$

Hence, although the transformation $C^{+}_{3,q}$ is defined on the set of natural numbers $\mathbb{N}$, its extension to negative integers $\mathbb{Z}$ preserves the same sign-symmetric structure. From this perspective, both the generalized problem in the form $C^{\pm}_{\kappa,q}$ and its inverse counterpart have received only limited attention in the literature, except for the partial studies reported in [9, 10].

1.2 Preliminaries and notation

1.2.1 Generalized Jacobsthal transformations

Definition 1.1 (Generalized Jacobsthal Numbers)**.** *The generalized Jacobsthal numbers are defined as follows:*

$$J^{\pm}_{\kappa,\theta,n} = \frac{\theta \cdot 2^n \pm (-1)^n}{\kappa}, \qquad (2 \nmid \theta,\ n \in \mathbb{N}_0 = \mathbb{N} \cup \{0\}).$$

Definition 1.2 (Generalized Jacobsthal Transformation)**.** *The generalized Jacobsthal transformation is defined as follows*

$$JS^{\pm}_{\kappa,q} = \begin{cases} 2q, & q \equiv 0 \pmod 2, \\ J^{\pm}_{\kappa,\theta=q,n=0}, & q \equiv 1 \pmod 2, \end{cases} \qquad q \in \mathbb{N}_0 = \mathbb{N} \cup \{0\}. \tag{1.1}$$

Definition 1.3 (Residual form of the generalized Jacobsthal transformation)**.** *The residual form of the generalized Jacobsthal transformation, equivalent to Definition 1.2, is expressed as follows:*

$$JS^{\pm}_{\kappa,q} = \begin{cases} 2q, & q \equiv 0 \pmod 2, \\ \dfrac{q-1}{\kappa}, & q \equiv 1 \pmod 2,\ q \equiv 1 \pmod \kappa, \\ \dfrac{q+1}{\kappa}, & q \equiv 1 \pmod 2,\ q \equiv -1 \pmod \kappa, \\ \varnothing, & q \equiv 1 \pmod 2,\ q \equiv 0 \pmod \kappa. \end{cases} \qquad q \in \mathbb{N}_0.$$

Here, $q \equiv 0 \pmod 2$ denotes an even number and $q \equiv 1 \pmod 2$ an odd number.

In this context, the residual form represents the *closed-form* of the generalized Jacobsthal transformation.

Definition 1.4 (Generalized Collatz Function)**.** *The generalized Collatz function is defined as follows*

$$C^{+}_{\kappa,q} = \kappa \cdot q + 1, \qquad C^{-}_{\kappa,q} = \kappa \cdot q - 1. \tag{1.2}$$

Definition 1.5 (Generalized Collatz Conjecture)**.** *The generalized Collatz conjecture is defined as follows*

$$C^{\pm}_{\kappa,q} = \begin{cases} \dfrac{q}{2}, & q \equiv 0 \pmod 2, \\ \kappa q \pm 1, & q \equiv 1 \pmod 2, \end{cases} \qquad q \in \mathbb{N}. \tag{1.3}$$

When iterated on any initial value $q_0 \in \mathbb{N}$, the sequence eventually reaches a periodic cycle or a fixed point (Point attractor), Pas depending on κ.

1.2.2 Jacobsthal trees and nodes

The basis of the generalized problems (1.1) and (1.3) is provided by the generalized Jacobsthal numbers introduced in Definition 1.1, whose closed form was established in earlier works [9, 10].

They can be structured into two subclasses of integers:

$$m_{\kappa,\theta,n} = \frac{\theta \cdot 2^{n-1} - 1}{\kappa}, \qquad p_{\kappa,\theta,k} = \frac{\theta \cdot 2^{k-1} + 1}{\kappa}, \qquad n \in \mathbb{N}_{\text{even}},\ k \in \mathbb{N}_{\text{odd}}. \tag{1.4}$$

Whenever these quantities are integers, they generate a new odd parameter thus defining the branching nodes of the corresponding Jacobsthal tree.

$$\delta \in \mathbb{N}_{\text{odd}}, \qquad \delta = \begin{cases} m_{\kappa,\theta,n}, & \text{if } \theta \equiv 1 \pmod{\kappa} \quad (JS^{+}), \\ p_{\kappa,\theta,k}, & \text{if } \theta \equiv -1 \pmod{\kappa} \quad (JS^{-}). \end{cases}$$

For odd θ and indices $n \in \mathbb{N}_{\text{even}}$, $k \in \mathbb{N}_{\text{odd}}$,

$$m_{\kappa,\theta,n} \in \mathbb{N}_0 \iff \theta\, 2^n \equiv 1 \pmod{\kappa},$$

$$p_{\kappa,\theta,k} \in \mathbb{N}_0 \iff \theta\, 2^k \equiv -1 \pmod{\kappa},$$

The Jacobsthal numbers themselves were studied in [11, 12], and the authors pointed out their possible role in the Collatz problem. However, as shown in [9, 10], the numbers (1.4) form, at certain points of sequences, the so-called *branching nodes* of other sequences

$$\{\theta \cdot 2^n\}_{n=0}^{+\infty}$$

based on powers of two. Such a process develops as $n \to +\infty$, resulting in the formation of a so-called *graph tree*, as in [13]. In the inverse iteration direction, along the branches of the tree, Collatz sequences $(CS^{\pm}_{\kappa,q})$ are formed.

Definition 1.6 (Point attractor)**.** *A point attractor (PA) is an attractor of a dynamical system that consists of a single stationary point.*

In the periodic cycle that terminates a Collatz sequence $CS^{\pm}_{\kappa,q}$, this role PA is played by the smallest odd value q_O. In a non-periodic cycle with increasing sequences, the smallest odd value $q_O = 1$ is a pseudo-attractor (PA$_{ps}$).

Therefore, the corresponding generalized Collatz conjecture asserts that, for any initial value $q_0 \in \mathbb{N}_{\mathrm{PA}(\mathrm{PA}_{\mathrm{ps}})}$, the iterated sequence defined by

$$q_{n+1} = C^{\pm}_{\kappa,q_0}$$

eventually reaches the set $\mathrm{PA}(\mathrm{PA}_{\mathrm{ps}})$.

Remark 1.7. *In the classical Collatz model with $\kappa = 3$ and $C(x) = 3x+1$, the periodic attractor is $PA = \{1\}$ for all $q \in \mathbb{N}$. In the case of $C(x) = 3x-1$, one obtains $PA = \{1,5,17\}$; for $C(x) = 5x+1$, $PA = \{1,13,17\}$; and for $C(x) = 181x+1$, $PA = \{1,27,35\}$.*

Definition 1.8 (Node)**.** *A node is a point of the sequence*

$$\{\theta 2^n\}_{n=0}^{+\infty}$$

that corresponds to the numbers $m_{\kappa,\theta,n}$ or $p_{\kappa,\theta,n}$ defined in (1.4).

The points of sequences $\{\theta \cdot 2^n\}_{n=0}^{+\infty}$ with numbers $m_{\kappa,\theta,n}$ or $p_{\kappa,\theta,n}$ correspond to the so-called nodes, from which other sequences branch, if the parameter θ is not a multiple of κ. If θ is a multiple of κ ($\theta = \theta_\kappa$), then the numbers $m_{\kappa,\theta,n}$ (or $p_{\kappa,\theta,n}$) are not integers, so no branching nodes are generated.

An illustration of nodes with $m_{\kappa,\theta,n}$ numbers is shown in Figure 1.1.

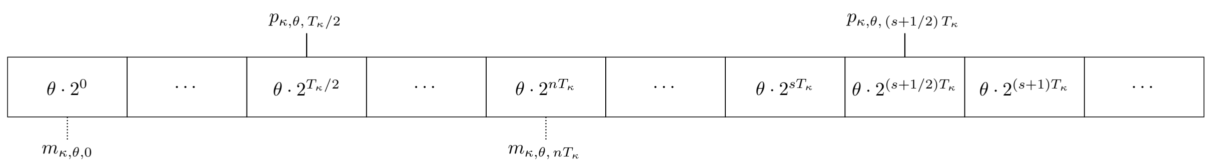

Figure 1.1. Arrangement of the numbers $m_{\kappa,\theta,n}$ (even indices, below) and $p_{\kappa,\theta,k}$ (odd indices, above) along the sequence $\theta \cdot 2^n$. If the values $m_{\kappa,\theta,n}$ and $p_{\kappa,\theta,k}$ are not integers (see Eq. (1.4) and Table 2.2), no nodes are defined.

Definition 1.9 (Period of the Nodes)**.** *The period of the nodes T_κ in the sequence*

$$\{\theta 2^n\}_{n=0}^{+\infty}$$

is the distance, in powers of 2^n, between two successive nodes of the same type.

Definition 1.10 (Jacobsthal tree)**.** *A Jacobsthal tree is the branching structure generated by the graph nodes of Jacobsthal sequences along increasing powers of two.*

Definition 1.11 (Sets of numbers associated with the Jacobsthal tree)**.** *The sets associated with the Jacobsthal tree are defined as follows.*

The graph tree rooted at the point attractor PA corresponds to the combined set consisting of odd numbers $N_{\kappa,PA,O}$ as nodes and even numbers $N_{\kappa,PA,E}$ as edges:

$$N_{\kappa,PA} = \bigcup_{i=1}^{k} N_{\kappa,PA,i} \;\cup\; \bigcup_{i=1}^{k} N_{\kappa,E,i}.$$

Definition 1.12 (Total stopping time (tst))**.** *We define the total stopping time tst as follows [14].*

In the Jacobsthal tree, the discrete time variable tst corresponds to the number of iterations ($n = tst$). Therefore, in the forward direction $n \to +\infty$, the time tst increases, while in the reverse construction of the Collatz sequence, tst decreases.

1.2.3 Structural interpretation

Informally, the proposed framework may be viewed as follows: Starting from root sequences of the form $\theta 2^n$, certain values generate integer branching nodes through the generalized Jacobsthal relations. These nodes form tree-like structures, called Jacobsthal trees, whose reverse trajectories correspond to generalized Collatz-type sequences. In this representation, periodicity properties of the nodes induce structural regularities in the associated $\kappa x \pm 1$ dynamics.

2. Main Results

2.1 Generalized Collatz and Jacobsthal transformations

In the forward direction ($n \to +\infty$), at nodes of the form $\{\delta\, 2^n\}_{n\geq 0}$ with $\delta \in \{m_{\kappa,\theta,n},\, p_{\kappa,\theta,n}\}$ whenever they are integers, other sequences branch.

In the reverse direction ($n \to 0$), using the relations

$$\kappa m_{\kappa,\theta,n} + 1 = \theta\, 2^n, \qquad \kappa p_{\kappa,\theta,k} - 1 = \theta\, 2^k, \qquad n \in \mathbb{N}_{\text{even}},\; k \in \mathbb{N}_{\text{odd}} \tag{2.1}$$

the segments $\{\delta 2^n\}_{n=1}^{\ell}$ merge at the nodes, forming Collatz-type sequences $CS^{\pm}_{\kappa,q}$.

Therefore, for every κ, the Collatz functions can be expressed as

$$C^{+}_{\kappa,q} = \kappa m_{\kappa,\theta,n} + 1, \qquad C^{-}_{\kappa,q} = \kappa p_{\kappa,\theta,k} - 1. \tag{2.2}$$

A similar reasoning applies to the system of nodes with numbers $p_{\kappa,\theta,k}$, leading to the mirror counterpart Collatz function $C^{-}_{\kappa,q}$. In this case,

$$p_{\kappa,\theta,k} = \frac{\theta\, 2^k + 1}{\kappa} \iff \theta\, 2^k = \kappa p_{\kappa,\theta,k} - 1, \qquad C^{-}_{\kappa,q} = \kappa p_{\kappa,\theta,k} - 1. \tag{2.3}$$

In justifying formulas (2.1)–(2.3), no additional constraints were imposed; therefore, both models $C^{\pm}_{\kappa,q}$ are structurally equivalent for all κ.

Thus, the Collatz-type problem can be generalized as

$$C^{\pm}_{\kappa,q} = \begin{cases} \dfrac{q}{2}, & \text{if } q \equiv 0 \pmod 2, \\ \kappa \cdot q \pm 1, & \text{if } q \equiv 1 \pmod 2, \end{cases} \qquad n \to 0, \tag{2.4}$$

and the reverse (Jacobsthal-type) problem as

$$JS^{\mp}_{\kappa,q} = \begin{cases} 2q, & q \equiv 0 \pmod 2, \\ \dfrac{q \pm 1}{\kappa}, & q \equiv 1 \pmod 2, \end{cases} \qquad n \to +\infty. \tag{2.5}$$

Since the graph tree serves as the basis for forming Collatz sequences, problem (2.4) should be considered as the direct problem, and (2.5) as the inverse problem of number transformation.

2.2 Examples of Jacobsthal trees

At the end of the article, an alternative formulation of a Collatz-type hypothesis is proposed.

To identify the transformed nodes, we distinguish two families:

- Nodes of type $m_{3,q,n}$ (for JS^{+}), defined as

$$m_{3,q,n} = \frac{q \cdot 2^n - 1}{3}, \qquad \text{defined whenever the numerator is divisible by 3.}$$

- Nodes of type $p_{3,q,n}$ (for JS^{-}), defined as

$$p_{3,q,n} = \frac{q \cdot 2^n + 1}{3}, \qquad \text{defined whenever the numerator is divisible by 3.}$$

Thus, we evaluate $J^{\pm}_{3,q,n}$ for q in the range 1 to 9. For $q = 1$, the corresponding values are shown in Table 2.1.

Therefore, in model (1.4), the numbers $J^{-}_{3,1,n}$, unlike $J^{+}_{3,1,n}$, are divisible by $3, 9, 15, 21, \ldots$. However, both numbers $J^{\pm}_{3,1,n}$ are divisible by 5. Thus, $J^{+}_{3,1,n}$ generate numbers $p_{3,1,n}$, while $J^{-}_{3,1,n}$ generate numbers $m_{3,1,n}$, thereby ensuring non-overlap of the subsets of numbers $m_{3,1,n}$ and $p_{3,1,n}$.

The numbers $J^{+}_{3,1,n}$ are not integers, whereas $J^{-}_{3,1,n} = J^{-}_{1,1,n}/3$ are integers. Therefore, numbers $m_{3,1,n}$ and $p_{3,1,n}$ are obtained by bisection of $J^{-}_{3,1,n}$, thereby guaranteeing that the sequences $CS^{\pm}_{3,q}$ terminate in unity.

For $\kappa > 1$, the numbers $J^{\pm}_{\kappa,1,n}$ are generated differently. For example, if

$$m_{5,1,n} = \frac{J^{-}_{1,1,n}}{5}, \quad \text{and} \quad p_{5,1,n} = \frac{J^{+}_{1,1,n}}{5},$$

then

$$m_{7,1,n} = \frac{J^-_{1,1,n}}{7}$$

are generated by uniting the sequences $J^+_{7,1,n} \cup J^-_{7,1,n}$, whereas the numbers $p_{7,1,n}$ are not integers. The case $\kappa = 9$ is analogous to $\kappa = 3$.

n	0	1	2	3	4	5	6	7	8	9	10	11	12	
$J^+_{1,1,n}$	2	1	5	7	17	31	65	127	257	511	1025	2047	4097	$p_{1,1,n} = 2n - 1$
$J^-_{1,1,n}$	0	3	3	9	15	33	63	129	255	513	1023	2049	4095	$m_{1,1,n} = 2n + 1$
$J^-_{3,1,n} = J^-_{1,1,n}/3$	0	1	1	3	5	11	21	43	85	171	341	683	1365	$m(p)_{3,1,n}$
$J^+_{5,1,n} = J^+_{1,1,n}/5$			1				13				205			$p_{5,1,n}$
$J^-_{5,1,n} = J^-_{1,1,n}/5$	0				3				51				819	$m_{5,1,n}$
$J^+_{7,1,n} = J^+_{1,1,n}/7$				1						73				
$J^-_{7,1,n} = J^-_{1,1,n}/7$	0						9						585	$m_{7,1,n}$
$J^-_{7,1,n} \cup J^+_{7,1,n}$	0			1			9			73			585	
$J^-_{9,1,n} = J^-_{1,1,n}/9$	0			1			7			57			455	$m(p)_{9,1,n}$

Table 2.1. Computed values of $J^{\pm}_{3,q,n}$ for the transformation model $C^{\pm}_{3,q}$ within the range $q = 1,\dots,9$. Highlighted rows in yellow indicate subsequences corresponding to $q = 1,3,5,7,9$. The rightmost column provides the associated generating expressions $p_{3,1,n}$ and $m_{3,1,n}$, defining the mappings $q \mapsto 3q \pm 1$.

If $q > 1$, divisibility by three among the numbers $J^{\pm}_{1,q,n}$ is selective: certain numbers $J^{\pm}_{1,3,n}$ are not divisible by three, so the non-integer numbers are $p_{3,3,n}$ and $m_{3,3,n}$, as are the numbers $p_{\kappa,q=\kappa}, n$ and $m_{\kappa,q=\kappa}, n$.

The correlation of numbers $m_{\kappa,q,n}$ and $p_{\kappa,q,n}$ with $J^{\pm}_{\kappa,1,n}$ is displayed in the right column of Table 2.1.

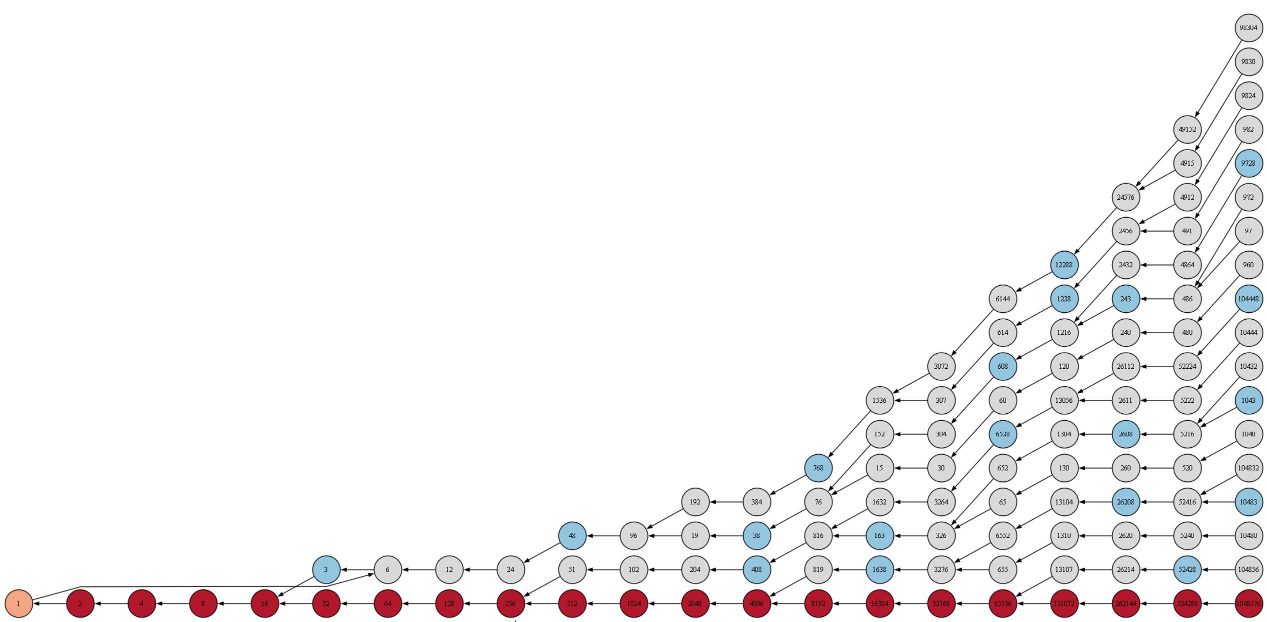

Figure 2.1. Representation of the Jacobsthal tree $J^+_{5,q}$, branching as $n \to +\infty$. In the reverse direction, the arrows indicate the trajectories of the Collatz sequences $C^+_{5,q}$ formed from the initial numbers in the columns.

2.3 Structural interpretation of the trees

Transformations (2.4) and (2.5) are inverse to each other in such a way that, as $n \to +\infty$ of graph (2.5), branching occurs in the form of a tree (the Jacobsthal tree), as shown in Figure 2.1 for the $J^+_{5,q}$ tree.

In the reverse direction $n \to 0$, sequences $CS^+_{5,q}$ are formed that converge along the branches of the tree toward the root

$$\{2^n\}_{n=0}^{+\infty}$$

sequence. The sequences $CS^{+}_{5,q}$ with initial numbers belonging to one column have the same total stopping time and the same *tst* time. These regularities hold true for other models of κ-conjectures. Therefore, as $tst \to +\infty$, the tree formation process described below is unambiguous, since each value of tst corresponds to a definite number and a list of numbers in the columns, for which the sequences $CS^{\pm}_{\kappa,q}$ have the same length. The inverse mapping is non-unique, since for the same number of iterations (or time tst), the unit value is reached by the sequences $CS^{\pm}_{\kappa,q}$ of numbers in the entire column.

Since the set of initial numbers is fixed/defined, their sequences $CS^{\pm}_{\kappa,q}$ reach the attractor (or pseudo-attractor) in the same number of iterations.

2.4 Periodicity theorem

We now formulate the main structural results of problems (2.4) and (2.5).

Theorem 2.1. *For all κ, the nodes located at points of the sequences $\{\theta \cdot 2^n\}_{n=0}^{+\infty}$ are periodic with period T_κ with respect to powers of two, while the numbers $m_{\kappa,\theta,n}$ and $p_{\kappa,\theta,n}$, as well as those of the neighbouring nodes, satisfy the linear relations*

$$2^{T_\kappa} = 1 + \kappa m_{\kappa,1,T_\kappa}, \tag{2.6a}$$

$$m_{\kappa,\theta,n+T_\kappa} = 2^{T_\kappa} m_{\kappa,\theta,n} + m_{\kappa,1,T_\kappa}, \tag{2.6b}$$

$$p_{\kappa,\theta,n+T_\kappa} = 2^{T_\kappa} p_{\kappa,\theta,n} - m_{\kappa,1,T_\kappa}, \tag{2.6c}$$

where $m_{\kappa,1,T_\kappa}$ denotes the first odd number of the root sequence $\{1 \cdot 2^n\}_{n=0}^{+\infty}$.

2.5 Periodic node formation

We verify formula (2.6a) as follows:

κ	1	3	5	7	9	11	13	15	17	19	21	23	25	27	29
$m_{\kappa,1,n}$	1	1	3	1	7	93	315	1	15	13 797	3	89	41 943	9 709	9 256 395
$p_{\kappa,1,k}$				f				f			f	f	f		
T_κ	1	2	4	3	6	10	12	4	8	18	6	11	20	18	28

κ	31	33	181
$m_{\kappa,1,n}$	1	31	8 466 826 192 629 220 211 924 569 210 775 188 859 772 039 349 080 675
$p_{\kappa,1,k}$	f		f
T_κ	5	10	180

Table 2.2. Values of $m_{\kappa,1,T_\kappa}$ and periods T_κ for selected values of κ.

The gray-shaded blocks indicate triplets of parameters κ, $\kappa+2$, and $m_{\kappa+2,1,T_\kappa}$ satisfying

$$\kappa = m_{\kappa+2,1,T_\kappa} \qquad \text{and} \qquad T_\kappa = \frac{T_{\kappa+2}}{2}.$$

From (2.6), if the period T_κ is odd, as in the cases $\kappa = 7, 23, 31, 47, 49, \ldots$, then the quantities $p_{\kappa,\theta,n}$ are not integers.

However, numbers $p_{\kappa,\theta,n}$ can take non-integer values for even period values as in the cases $\kappa = 35, 39, 45, 51, \ldots$.

Remark 2.2. *From formula (2.6a) we have $2^{T_\kappa} - 1 = \kappa \cdot m_{\kappa,1,T_\kappa}$. Therefore, the factorization of $2^{T_\kappa} - 1$ can be expressed in the form of binary products of the type $\kappa \cdot m_{\kappa,1,T_\kappa}$.*

We now justify formula (2.6b). From Figure 2.2(a), the node numbers $p_{\kappa,\theta,n}$ and $m_{\kappa,\theta,n}$ are used to denote the two corresponding families of sequence elements.

The transformations for both can be written as:

$$\theta \cdot 2^n = \kappa \cdot p_{\kappa,\theta,n} - 1, \qquad \theta \cdot 2^{n+T_\kappa} = \kappa \cdot p_{\kappa,\theta,n+T_\kappa} - 1.$$

Therefore, for the odd numbers:

$$\kappa \cdot p_{\kappa,\theta,n} - 1 = \frac{\kappa \cdot p_{\kappa,\theta,n+T_\kappa} - 1}{2^{T_\kappa}},$$

or equivalently:

$$p_{\kappa,\theta,n+T_\kappa} = 2^{T_\kappa} p_{\kappa,\theta,n} - m_{\kappa,1,T_\kappa}.$$

For the even numbers, the analogous relation is:

$$\theta \cdot 2^n = \kappa \cdot m_{\kappa,\theta,n} + 1, \qquad \theta \cdot 2^{n+T_\kappa} = \kappa \cdot m_{\kappa,\theta,n+T_\kappa} + 1,$$

leading to

$$m_{\kappa,\theta,n+T_\kappa} = 2^{T_\kappa} m_{\kappa,\theta,n} + m_{\kappa,1,T_\kappa}.$$

Here, $p_{\kappa,1,T_\kappa}$ and $m_{\kappa,1,T_\kappa}$ denote the first odd and even nodes of the corresponding root sequences $\{1 \cdot 2^n\}_{n=0}^{n=+\infty}$.

We present the analytical forms of formulas (2.6b) within the range of values $\kappa = 1$ to 9.

κ	1	3	5	7	9	181
$m_{\kappa,\theta,n+T_\kappa}$	$2^1 m_{1,\theta,n} + 1$	$2^2 m_{3,\theta,n} + 1$	$2^4 m_{5,\theta,n} + 3$	$2^3 m_{7,\theta,n} + 1$	$2^6 m_{9,\theta,n} + 7$	$2^{180} m_{181,\theta,n}$ $+ 84\,668\,261\,926\,292\,202$ $11\,924\,569\,210\,775\,188$ $859\,772\,039\,349\,080\,675$

Table 2.3. Examples of recurrence relations of type (2.6b) for selected values of κ.

2^n	$m_{1,1,n}$	$m_{3,1,n}$	$m_{5,1,n}$	$m_{7,1,n}$	$m_{9,1,n}$	$m_{11,1,n}$	$m_{13,1,n}$	$m_{15,1,n}$	$m_{17,1,n}$	$m_{19,1,n}$	$m_{21,1,n}$	$m_{23,1,n}$
2^{20}	1 048 575	349 525	29 715			95 325		69 905				
2^{19}	524 287											
2^{18}	262 143	87 381		37 449	29 127					13 797	12 483	
2^{17}	13 107											
2^{16}	65 535	21 845	13 107					4 369	3 855			
2^{15}	32 767			4 681								
2^{14}	16 383	5 461										
2^{13}	8 191											
2^{12}	4 095	1 365	819	585	455		315	273			195	
2^{11}	2 045											89
2^{10}	1 023	341				93						
2^{9}	511			73								
2^{8}	255	85	51					17	15			
2^{7}	127											
2^{6}	63	21		9	7						3	
2^{5}	31											
2^{4}	15	5	3					1				
2^{3}	7			1								
2^{2}	3	1										
2^{1}	1											
2^{0}	0	0	0	0	0	0	0	0	0	0	0	0

Table 2.4. Illustration of the node formation property with the numbers $m_{\kappa,1,n}$ for $\kappa = 1$ to $\kappa = 9$.

The periodicity of node formation with numbers $m_{\kappa,\theta,n}$ is shown in Table 2.4, where the values of the first odd numbers $m_{\kappa,1,T_\kappa}$ in formula (2.6a) are highlighted in yellow.

The period T_κ also correlates with the total stopping time tst, as shown in Table 2.5 for the transformation function $C^+_{5,q}$ $(T_5 = 4)$.

$m_{5,1,n}$	0	3	51	819	13 107	209 715
$tst + T_5$	1	$1+4$	$5+4=9$	$9+4=13$	$13+4=17$	$17+4=21$
		5	9	13	17	21

Table 2.5. Example of computed values for $m_{5,1,n}$ and increments by T_5.

Taking into account the structure of the nodes in Figure 1.1, for the numbers $p_{\kappa,\theta,n+T_\kappa}$ as shown in Table 2.3, the results are analogous, except with a minus sign.

In (2.6b), the first formula

$$m_{3,\theta,n+2} = 4m_{3,\theta,n} + 1$$

is known [15].

The corresponding relations for other values of κ were previously investigated in [9].

Formulas of type (2.6b) are justified as $n \to +\infty$, i.e., they reflect regularities in the transformation of parameterized θ odd Jacobsthal numbers $m_{\kappa,\theta,n}$ and $p_{\kappa,\theta,n}$.

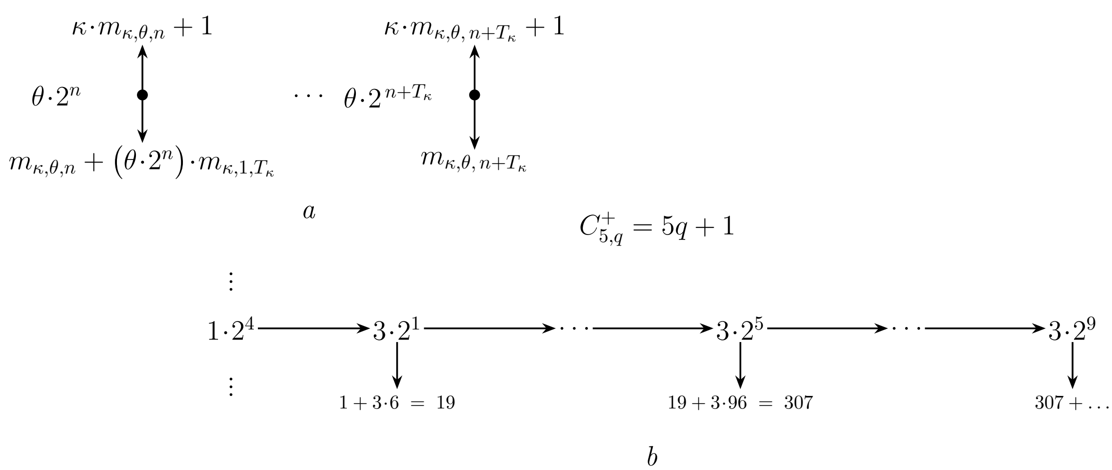

Figure 2.2. (a) Generalized graph associated with (2.4) and (2.5); (b) Graph associated with (2.5).

2.6 Structural properties of node transformations

Property 2.3. *For all κ, the difference between two numbers that are adjacent in period T_κ is proportional to the transformation function of odd numbers $C^\pm_{\kappa,q}$:*

$$\begin{cases} m_{\kappa,\theta,n+T_\kappa} - m_{\kappa,\theta,n} = m_{\kappa,1,T_\kappa}\left(\kappa m_{\kappa,\theta,n} + 1\right) = m_{\kappa,1,T_\kappa} C^+_{\kappa,q}, \\ p_{\kappa,\theta,n+T_\kappa} - p_{\kappa,\theta,n} = m_{\kappa,1,T_\kappa}\left(\kappa p_{\kappa,\theta,n} - 1\right) = m_{\kappa,1,T_\kappa} C^-_{\kappa,q}. \end{cases}$$

Proof. From (2.6b), we have

$$m_{\kappa,\theta,n+T_\kappa} - m_{\kappa,\theta,n} = (2^{T_\kappa} - 1)m_{\kappa,\theta,n} + m_{\kappa,1,T_\kappa}.$$

Using (2.6a), namely

$$2^{T_\kappa} - 1 = \kappa m_{\kappa,1,T_\kappa},$$

we obtain

$$m_{\kappa,\theta,n+T_\kappa} - m_{\kappa,\theta,n} = m_{\kappa,1,T_\kappa}\left(\kappa m_{\kappa,\theta,n} + 1\right) = m_{\kappa,1,T_\kappa} C^+_{\kappa,q}.$$

Similarly, from (2.6c),

$$p_{\kappa,\theta,n+T_\kappa} - p_{\kappa,\theta,n} = (2^{T_\kappa} - 1)p_{\kappa,\theta,n} - m_{\kappa,1,T_\kappa}.$$

Using again (2.6a), we obtain

$$p_{\kappa,\theta,n+T_\kappa} - p_{\kappa,\theta,n} = m_{\kappa,1,T_\kappa}\left(\kappa p_{\kappa,\theta,n} - 1\right) = m_{\kappa,1,T_\kappa} C^{-}_{\kappa,q}.$$

□

Property 2.4. *For any κ, the following identities hold:*

$$\begin{cases} m_{\kappa,\theta,n} + p_{\kappa,\theta,n+T_\kappa/2} = \dfrac{\theta\, 2^n}{\kappa}\left(1 + 2^{T_\kappa/2}\right), & \textit{if the numbers } p_{\kappa,\theta,n} \textit{ are integers},\\ -m_{\kappa,\theta,n} + m_{\kappa,\theta,n+T_\kappa} = \theta\, 2^n m_{\kappa,1,T_\kappa}, & \textit{if the numbers } p_{\kappa,\theta,n+T_\kappa} \textit{ are not integers}. \end{cases}$$

Proof. From (2.1), we have:

$$m_{\kappa,\theta,n} + p_{\kappa,\theta,n+T_\kappa/2} = \frac{\theta\cdot 2^n - 1}{\kappa} + \frac{\theta\cdot 2^n \cdot 2^{T_\kappa/2} + 1}{\kappa} = \frac{\theta\cdot 2^n}{\kappa}\left(1 + 2^{T_\kappa/2}\right),$$

and

$$-m_{\kappa,\theta,n} + m_{\kappa,\theta,n+T_\kappa} = \frac{-\theta\cdot 2^n + 1}{\kappa} + \frac{\theta\cdot 2^n\cdot 2^{T_\kappa} - 1}{\kappa} = \frac{\theta\cdot 2^n}{\kappa}\left(-1 + 2^{T_\kappa}\right) = \theta 2^n m_{\kappa,1,T_\kappa}.$$

□

Property 2.5. *For all κ, the asymptotic ratios satisfy*

$$\lim_{n\to+\infty} \frac{m_{\kappa,\theta,n+T_\kappa}}{m_{\kappa,\theta,n}} = 2^{T_\kappa},$$

$$\lim_{n\to+\infty} \frac{p_{\kappa,\theta,n+T_\kappa}}{p_{\kappa,\theta,n}} = 2^{T_\kappa}.$$

Proof. From the periodicity relations (2.6b) and (2.6c), we have

$$m_{\kappa,\theta,n+T_\kappa} = 2^{T_\kappa} m_{\kappa,\theta,n} + m_{\kappa,1,T_\kappa},$$

and

$$p_{\kappa,\theta,n+T_\kappa} = 2^{T_\kappa} p_{\kappa,\theta,n} - m_{\kappa,1,T_\kappa}.$$

Dividing the first identity by $m_{\kappa,\theta,n}$ gives

$$\frac{m_{\kappa,\theta,n+T_\kappa}}{m_{\kappa,\theta,n}} = 2^{T_\kappa} + \frac{m_{\kappa,1,T_\kappa}}{m_{\kappa,\theta,n}}.$$

Since $m_{\kappa,\theta,n} \to +\infty$ as $n \to +\infty$, the second term tends to zero. Hence,

$$\lim_{n\to+\infty} \frac{m_{\kappa,\theta,n+T_\kappa}}{m_{\kappa,\theta,n}} = 2^{T_\kappa}.$$

Similarly, dividing the second identity by $p_{\kappa,\theta,n}$ gives

$$\frac{p_{\kappa,\theta,n+T_\kappa}}{p_{\kappa,\theta,n}} = 2^{T_\kappa} - \frac{m_{\kappa,1,T_\kappa}}{p_{\kappa,\theta,n}}.$$

Since $p_{\kappa,\theta,n} \to +\infty$ as $n \to +\infty$, the second term also tends to zero. Therefore,

$$\lim_{n\to+\infty} \frac{p_{\kappa,\theta,n+T_\kappa}}{p_{\kappa,\theta,n}} = 2^{T_\kappa}.$$

□

2.7 Partition properties

Property 2.6. *For a given κ we have:*

$$\text{If } \theta \neq \delta, \text{ then } \begin{cases} m_{\kappa,\theta,n} \neq m_{\kappa,\delta,\nu}, \\ p_{\kappa,\theta,n} \neq p_{\kappa,\delta,\nu}. \end{cases}$$

Proof. Assume that

$$m_{\kappa,\theta,n} = m_{\kappa,\delta,\nu}.$$

Then, from (2.1),

$$\theta \cdot 2^n = \delta \cdot 2^\nu,$$

which implies

$$\frac{\theta}{\delta} = 2^{\nu-n}.$$

Since both θ and δ are odd, the ratio θ/δ cannot be a nontrivial power of two. Therefore,

$$\theta = \delta \quad \text{and} \quad n = \nu,$$

which contradicts the assumption $\theta \neq \delta$. Hence,

$$m_{\kappa,\theta,n} \neq m_{\kappa,\delta,\nu}.$$

The proof for the family $p_{\kappa,\theta,n}$ is analogous.

Therefore, the sets $S(m_{\kappa,\theta,n})$ and similarly $S(p_{\kappa,\theta,n})$, contain no identical elements.

□

2.8 Closed cycles and pseudo-attractors

In the classical Collatz sequence, the sequence $CS^+_{3,q}$ converges to a periodic cycle with a unit smallest odd value ($q_o = 1$). Conjectures $C^-_{3,q_o} = 3q_o - 1$, $C^+_{5,q_o} = 5q_o + 1$, $C^+_{181,q_o} = 181q_o + 1$, are known [16–21], in which the sequence $CS^{\pm}_{\kappa,q}$ converges to a periodic cycle with minimal $q_o > 1$, or grows without bound if $q_o \geq 5$, as shown in Table 2.6.

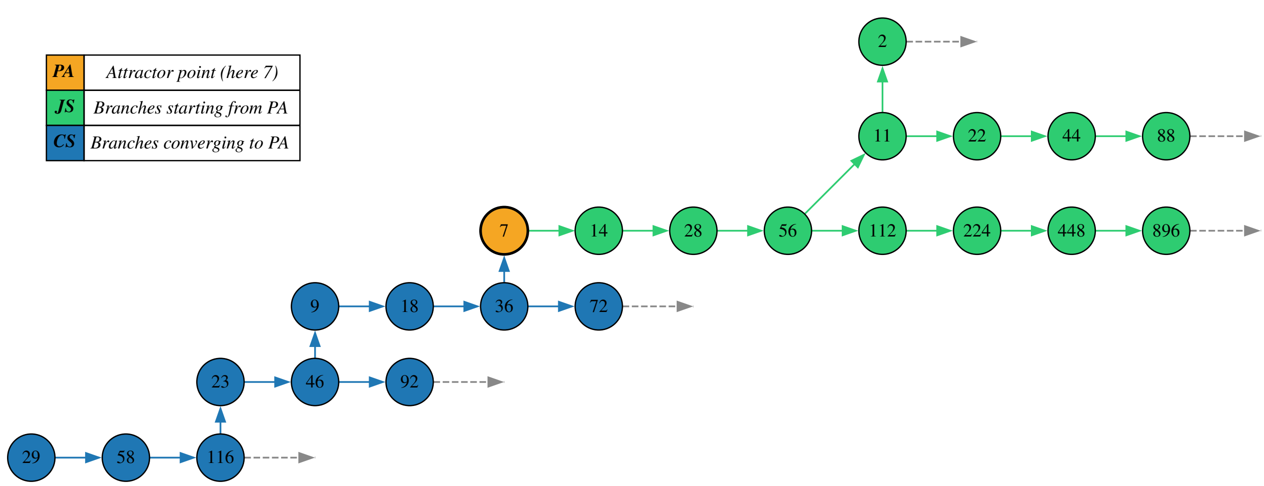

Figure 2.3. The graphs of the sequences $JS^-_{5,q}$ (in the arrow direction) and $CS^+_{5,q}$ (in the reverse direction).

Cases with divergent trajectories correspond to increasing sequences $CS^{\pm}_{\kappa,q}$.

κ	$C^{\pm}_{\kappa,q_0}$	PA	Type of cycle	$PA_\kappa = \sum_{i=0}^{k-1} \frac{\kappa^{k-v-1}\,2^v}{2^\ell - \kappa^k}$	$\mathbb{N}_{(\pm,\kappa,PA)}$	$\mathbb{N}_{(\pm,\kappa,PA)}/\mathbb{N}$
1	C^{+}_{1,q_0}	1	$\to 1 \to 0$	$PA_1 = 1/(3^1 \cdot 2^1) = 1$	$\mathbb{N}_{(+,1,1)}$	–
	C^{-}_{1,q_0}	1	$\to 1 \to 2 \to 1 \to \cdots$	$PA_1 = 1/(3^1 - 2^1) = 1$	$\mathbb{N}_{(-,1,1)}$	–
3	C^{+}_{3,q_0}	1	$\to 1 \to 4 \to 2 \to 1 \to \cdots$	$PA_3 = 1/(2^2 - 3^1) = 1$	$\mathbb{N}_{(+,3,1)}$	1
	$C^{-}_{3,q}$	1	$\to 1 \to 2 \to 1 \to \cdots$	$PA_3 = 1/(3^1 - 2^2) = 1$	$\mathbb{N}_{(-,3,1)}$	**32.77%**
		5	$\cdots \to 5 \to 7 \to 5 \to \cdots$	$PA_3 = (3^1 + 2^1)/(3^2 - 2^3) = 5$	$\mathbb{N}_{(-,3,5)}$	**32.34%**
		17	$\to 17 \to 25 \to 37 \to 55 \to 41 \to 61 \to 91 \to 17 \to \cdots$	$PA_3 = \frac{3^6 + \cdots + 2^{11}}{3^7 - 2^{11}} = \frac{2363}{139} = 17$	$\mathbb{N}_{(-,3,17)}$	**34.90%**
5	C^{-}_{5,q_0}	1	$\cdots \to 1 \to 1 \to \cdots$	$PA_5 = 1/(5^1 - 2^2) = 1$	$\mathbb{N}_{(-,5,1)}$	–
		∞	$\to 1 \to \infty \to \cdots$	–	$\mathbb{N}_{(-,5,\infty)}$	–
	C^{+}_{5,q_0}	1	$\cdots \to 1 \to 3 \to 1 \to \cdots$	$PA_5 = \frac{5^1 + 2^1}{2^5 - 3^2} = 7/7 = 1$	$\mathbb{N}_{(+,5,1)}$	**0.58%**
		13	$\cdots \to 13 \to 33 \to 83 \to 13 \to \cdots$	$PA_5 = \frac{5^2 + 2^1 \cdot 5^1 + 2^2}{2^7 - 5^3} = 39/3 = 13$	$\mathbb{N}_{(+,5,13)}$	**0.86%**
		17	$\cdots \to 17 \to 43 \to 27 \to 17 \to \cdots$	$PA_5 = \frac{5^2 + 2^1 \cdot 5^1 + 2^4}{2^7 - 5^3} = 51/3 = 17$	$\mathbb{N}_{(+,5,17)}$	**5.79%**
		$PA_{ps} = 7$	$\cdots \to \infty \to \cdots$	–	$\mathbb{N}_{(+,5,\infty)}$	**92.77%**
181	C^{+}_{181,q_0}	1	$\cdots \to 1 \to \infty$	–	$\mathbb{N}_{(+,181,\infty)}$	–
		27	$\cdots \to 27 \to 611 \to 27 \to \cdots$	$PA_{181} = \frac{181 + 2^5}{2^{15} - 181^2} = 27$	$\mathbb{N}_{(+,181,27)}$	–
		35	$\cdots \to 35 \to 99 \to 35 \to \cdots$	$PA_{181} = \frac{181 + 2^6}{2^{15} - 181^2} = 35$	$\mathbb{N}_{(+,181,35)}$	–
	C^{-}_{181,q_0}	1	$\cdots \to 1 \to \infty$	–	$\mathbb{N}_{(-,181,\infty)}$	–

Table 2.6. Characteristics of the generalized transformations $C^{\pm}_{\kappa,q}$ with closed and open loops.

For these sequences, the trajectories are associated with the pseudo-attractor $PA_{ps} = 7$, corresponding to the node of the tree in Figure 2.3 generated by transformation (2.5) from the root sequence.

We see that as $n \to +\infty$ toward this point $\mathrm{PA_{ps}} = 7$, the trajectories $CS^{+}_{5,q}$ of the transformations of the initial doubled numbers $q = 7, 11, 15, \ldots$ converge.

However, the cycle is not closed, and therefore the point $\mathrm{PA_{ps}} = 7$ serves as a pseudo-attractor.

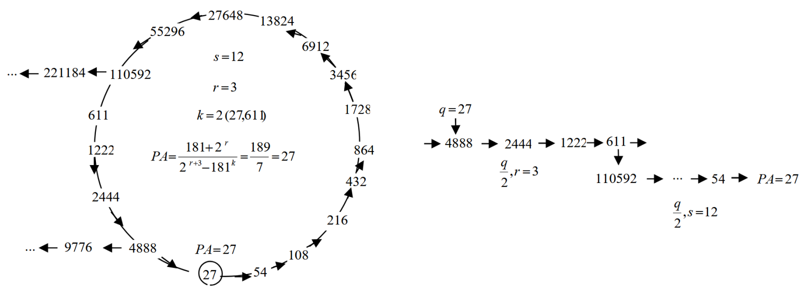

Figure 2.4. Examples of closed cycles with attractor $PA = 27$ corresponding to Collatz-type sequences.

2.9 Closed cycles and branching nodes

Property 2.7. *The number of branching nodes of the tree equals the number of odd numbers contained in a closed cycle with attractor PA.*

Proof. Consider a closed cycle of the transformation $C^{\pm}_{\kappa,q}$ containing the odd values

$$q_0, q_1, \ldots, q_{r-1}, \qquad q_r = q_0.$$

Between two consecutive odd values q_i and q_{i+1}, the iteration consists of one transformation

$$q \mapsto \kappa q \pm 1,$$

followed by a finite number $s_i \geq 1$ of divisions by 2. Hence,

$$q_{i+1} = \frac{\kappa q_i \pm 1}{2^{s_i}}.$$

Equivalently, in the inverse Jacobsthal construction,

$$q_i = \frac{q_{i+1} 2^{s_i} \mp 1}{\kappa}.$$

Thus, each transition from one odd value of the cycle to the next corresponds to one branching node in the associated Jacobsthal tree.

Since the cycle contains exactly r odd values, and since each of these values generates exactly one inverse transition before the cycle closes, the corresponding Jacobsthal tree contains exactly r branching nodes along the closed cycle.

□

3. Conclusion

We have developed a structural framework for generalized $\kappa x \pm 1$ transformations based on Jacobsthal sequences and their associated branching structures, which we call Jacobsthal trees. Within this representation, classical Collatz-type iterations appear as reverse trajectories along the branches of these trees. The periodicity of nodes, the recurrence relations governing their formation, and the structural identities derived in this work provide a unified description of the dynamics of $\kappa x \pm 1$ transformations. In particular, for a fixed κ, the natural numbers can be organized into disjoint subsets associated with distinct attractors or pseudo-attractors. Each Jacobsthal tree generates a set $N_{\kappa,PA}$ of odd nodes together with the corresponding even numbers $N_{\kappa,E}$, and these subsets appear to be mutually disjoint from the observed computational structures.

This motivates the following structural decomposition:

$$\mathbb{N} = \bigcup_{i=1}^{\nu} N_{\kappa,PA_i} \cup \bigcup_{i=1}^{\nu} N_{\kappa,E_i}.$$

Computational experiments performed on the first million initial values support this structural decomposition and confirm the observed non-intersection of subsets associated with different attractors.

The Jacobsthal-tree representation therefore provides an alternative structural viewpoint on generalized $\kappa x \pm 1$ discrete dynamical systems, highlighting intrinsic periodic symmetries and partition properties of the set $\mathbb{N}$.

Article Information

Author Contributions: Conceptualization: PK, DM; Methodology: PK, DM; Validation: PK, DM; Formal analysis: PK, DM; Investigation: PK, DM; Writing – original draft: PK, DM; Writing – review & editing: PK, DM; Project administration: DM.

Artificial Intelligence Statement: All mathematical results, definitions, proofs, computations, and scientific interpretations presented in this work were independently developed and validated by the authors. AI tools were used for language improvement, grammar correction, formatting assistance, and manuscript preparation. The authors take full responsibility for the content of this article.

Conflict of Interest Disclosure: The authors declare that they have no conflict of interest.

Plagiarism Statement: This article was scanned by the plagiarism program.

References

[1] D. Barina, *Improved verification limit for the convergence of the Collatz conjecture*, J. Supercomput., **81** (2025), Article ID 810. https://doi.org/10.1007/s11227-025-07337-0

[2] F. Kaplan, A. Özkoç Öztürk, *Binomial transforms of k-Narayana sequences and some properties*, Fundam. J. Math. Appl., **7**(3) (2024), 137–146. https://doi.org/10.33401/fujma.1468536

[3] S. Uygun, *Binomial transforms of k-Jacobsthal sequences*, J. Math. Comput. Sci., **7**(6) (2017), 1100–1114. https://doi.org/10.28919/jmcs/3474

[4] E. E. Kara, M. Ilkhan, *Some properties of generalized Fibonacci sequence spaces*, Linear Multilinear Algebra, **64**(11) (2016), 2208–2223. https://doi.org/10.1080/03081087.2016.1145626

[5] E. Olgac, *Topology and structure of directed acyclic graphs*, in: Future of Information and Communication Conference (FICC 2021), Adv. Intell. Syst. Comput., **1364** (2021). https://doi.org/10.1007/978-3-030-73103-8_23

[6] D. Bhattacharjee, *2-adic finite-certificate descent closure for the 3x+1 Collatz problem*, Preprint (2025). Available online: https://www.researchgate.net/publication/405077396_2-Adic_Finite-Certificate_Descent_Closure_for_the_3x1_Collatz_Problem

[7] M. B. Nathanson, *Permutation patterns of the iterated Syracuse function*, Integers, **24A** (2024), 1-24. Available online: https://math.colgate.edu/~integers/vol24a.html

[8] D. Mailland, P. Kosobutskyy, *Modelling the Collatz problem from a Jacobsthal viewpoint*, CDS, **8**(1) (2026), 49–55. https://doi.org/10.23939/cds2026.01.049

[9] P. Kosobutskyy, *The Jacobsthal-Collatz-Terras model of conjecture the natural numbers in $\kappa q+1$ problems*, J. Appl. Math., **3**(2) (2025), Article ID 1767. https://doi.org/10.59400/jam1767

[10] P. Kosobutskyy, O. Oborska, B. Vasylyshyn, *Jacobsthal recurrent numbers as a platform for transformations $\kappa q \pm 1$*, CDS, **7**(1) (2025), 288-299. https://doi.org/10.23939/cds2025.01.288

[11] A. Horadam, *Jacobsthal representation numbers*, Fibonacci Quart., **34**(1) (1996), 40–54.

[12] M. Pratsiovytyi, D. Karvatsky, *Jacobsthal–Lucas series and their applications*, Algebra Discrete Math., **24**(1) (2017), 169–180.

[13] M. Chamberland, *An update on the 3x+1 problem*, Working Paper, Department of Mathematics and Computer Science, Grinnell College (2003). Available online: https://chamberland.math.grinnell.edu/papers/3x_survey_eng.pdf

[14] R. Terras, *A stopping time problem on the positive integers*, Acta Arith., **30**(3) (1976), 241–252.

[15] P. Andolaro, *The 3x+1 problem and directed graphs*, Fibonacci Quart., **40**(1) (2002), 43–54.

[16] J. C. Lagarias, *The 3x+1 problem: An overview*, In: J. C. Lagarias (Ed.), The Ultimate Challenge: The 3x+1 Problem, Amer. Math. Soc., Providence, RI, 2010, 3–29.

[17] S. Volkov, *A probabilistic model for the 5k+1 problem and related maps*, Stochastic Process. Appl., **116**(4) (2006), 662–674. https://doi.org/10.1016/j.spa.2005.11.007

[18] R. Crandall, *On the 3x+1 problem*, Math. Comp., **32**(144) (1978), 1281–1292. https://doi.org/10.2307/2006353

[19] C. Sultanov, C. Koch, S. Cox, *Collatz sequences in the light of graph theory*, Preprint, Potsdam University Repository (2020). https://doi.org/10.25932/publishup-48214

[20] B. Snapp, M. Trac, *The Collatz problem and analogues*, J. Integer Seq., **11** (2008), Article ID 08.4.7.

[21] L. Green, *The negative Collatz sequence*, version 1.25, 14 Aug. 2022. Available online: https://aplusclick.org/pdf/neg_collatz.pdf